Available online at www.sciencedirect.com
SCIENCE DIRECT
Global and Planetary Change 52 (2006) 23–56
GLOBAL AND PLANETARY CHANGE
www.elsevier.com/locate/gloplacha

Characterization of Asian Dust during ACE-Asia☆

R. Arimoto [a,*], Y.J. Kim [b], Y.P. Kim [c], P.K. Quinn [d], T.S. Bates [d], T.L. Anderson [e], S. Gong [f], I. Uno [g], M. Chin [h], B.J. Huebert [i], A.D. Clarke [i], Y. Shinozuka [i], R.J. Weber [j], J.R. Anderson [k], S.A. Guazzotti [l], R.C. Sullivan [l], D.A. Sodeman [l], K.A. Prather [l], I.N. Sokolik [j]

[a] *Carlsbad Environmental Monitoring & Research Center, New Mexico State University, Carlsbad, NM 88220, USA*
[b] *Advanced Environmental Monitoring Research Center (ADEMRC), Department of Environmental Science and Engineering, Gwangju Institute of Science and Technology (GIST), Gwangju 500-712, Republic of Korea*
[c] *Department of Environmental Science and Engineering, Ewha Womans University, 11-1 Daehyundong, Seodaemungu, Seoul 120-750, Republic of Korea*
[d] *Pacific Marine Environmental Laboratory, National Oceanic and Atmospheric Administration, Seattle, WA 98115, USA*
[e] *Department of Atmospheric Sciences, University of Washington, Seattle, WA 98195, USA*
[f] *Air Quality Research Branch, Atmospheric Environment Service, Ontario, Canada M3H 5T4*
[g] *Research Institute for Applied Mechanics, Kyushu University Kasuga 816-8580, Fukuoka, Japan*
[h] *NASA Goddard Space Flight Center, Greenbelt, MD 20771, USA*
[i] *School of Ocean and Earth Science, University of Hawaii at Manoa, Honolulu, HI 96822, USA*
[j] *School of Earth and Atmospheric Sciences, Georgia Institute of Technology, Atlanta, GA 30332, USA*
[k] *Environmental Fluid Dynamics Program, Arizona State University, Tempe AZ 85287, USA*
[l] *Department of Chemistry and Biochemistry, University of California at San Diego, La Jolla CA 92093, USA*

Received 24 March 2005; accepted 9 February 2006
Available online 26 May 2006

Abstract

ACE-Asia was a multi-national collaboration organized to investigate and understand the chemistry, radiative properties, and climatic effects of mineral dust and other aerosol particles in the East Asia/Northwest Pacific region. Studies conducted at the Gosan and Zhenbeitai surface supersites show striking variations in aerosol concentrations and properties that were affected by the occurrence and origins of the Asian dust storms, air mass pathways, and mixing during the transport. Investigations conducted on the R/V Ronald H. Brown (RHB) showed that dust had a pervasive influence on the chemical composition, size distribution, and optical properties of the aerosol. Analyses using an aerosol time-of-flight mass spectrometer on the RHB showed that most of the coarse-particle nitrate and sulfate in post-frontal air was associated with dust, and more remarkably, that competitive or exclusionary processes evidently are involved in the uptake or production of these substances. Studies conducted onboard the NCAR C-130 aircraft showed that coarse-mode dust was less absorbing and less hygroscopic than pollution aerosol and that there was little correlation in light scattering and absorption by the sub- vs. super-micrometer aerosol. Below ~2 km, dust was commonly mixed with pollutants, and this had a stronger influence on the optical properties of the submicrometer particles than the coarse-mode dust; at higher altitudes, the dust was less affected by pollution. Single particle analyses of C-130 samples showed that the mixing of black carbon (BC) with dust was common, but only certain types of BC particles were aggregated. Models were used in the planning, execution and interpretative phases of ACE-Asia; and summaries of modeling results are presented to illustrate the

☆ Note: the author list is arranged in the sequence their contributions were received.

* Corresponding author.
E-mail address: arimoto@cemrc.org (R. Arimoto).

0921-8181/$ - see front matter © 2006 Elsevier B.V. All rights reserved.
doi:10.1016/j.gloplacha.2006.02.013

progress being made in identifying new dust sources; in depicting the time-varying, three-dimensional structure of dust plumes; and in quantifying the production, transport, and deposition of Asian dust.
© 2006 Elsevier B.V. All rights reserved.

Keywords: Asian dust; aerosols; chemistry; radiative effects; climate

1. Introduction

Several major outbreaks of atmospheric dust occurred during ACE-Asia, the Asian Pacific Regional Aerosol Characterization Experiment (Huebert et al., 2003), and these dust storms facilitated studies of the chemistry, radiative properties, and climatic effects of mineral dust and other types of aerosol particles (hereinafter simply "aerosols"). Indeed, the numbers of studies and programs focusing on the Asian aerosol have grown rapidly over the past 20 to 30 years as the importance of Asian outflow for regional climate and global biogeochemical cycles has become increasingly apparent.

This heightened interest in the Asian aerosol has been paralleled by advances in the methods used for characterizing aerosol properties and modeling the effects of aerosols on Earth systems. Despite these positive developments, the size of the region, the diversity of sources, and the complexity of the chemical and physical processes involved make it difficult to determine the extent to which human activities have perturbed the climate system. An equal if not greater challenge lies in developing a framework for reliably predicting how future climates may be affected by human activities and in developing the modeling tools needed to do so.

With recognition of these needs, a major objective for ACE-Asia was to strengthen the underpinnings of models being developed to predict the climatic responses to large-scale changes in aerosol composition and loadings over Asia. Therefore, one main goal of this summary is to bring together measurements of dust aerosol properties with modeling results and to highlight what was learned about the linkages between atmospheric dust and climate. The results presented here have been contributed by a group of collaborators who have conducted both field and modeling studies for the program. There are several limitations to the scope of this review that will soon become apparent to the reader, however. In particular, we do not consider in detail the information obtained from a network of lidars (the Asian Dust Network or ADNet, Shimizu et al., 2004) nor do we consider the information obtained from satellites (e.g., Wang et al., 2003).

While the focus of this paper is on the Asia/Pacific region, the results presented have global implications, not only because Asia is such a large dust source, but also because the approaches needed for assessing dust/chemistry/climate relationships transcend geographical region. Nevertheless, comparisons of results from ACE-Asia with studies in other regions have uncovered some basic differences in the properties of dust as highlighted below. Also relevant to assessing the broader human impacts on the dust cycle are the extensive studies of Chinese loess/paleoclimate relationships (Zhang, 1984; Liu et al., 1985; An et al., 1990; Porter, 2001) and the observations of Asian dust storm frequencies made during the last century (e.g., Sun et al., 2001; Natsagdorj et al., 2003; Zhang et al., 2003a,b). The former provide some perspective on the dust–climate interactions that operated before the Earth systems became perturbed by human activities. The more recent observations, on the other hand, are a first step for assessing how the changes in life-style and land-use practices occurring in Asia have affected the production of Asian dust. Both types of assessments have clear implications for other dust-producing regions.

2. Scientific uncertainties, issues, and questions

As interest has grown in the potential for climate forcing by aerosols, a seminal paper by Charlson et al. (1992) and a report issued shortly thereafter (IPCC, 1994) drew attention to the large uncertainties in the aerosols' direct radiative effects and the even larger uncertainties in the aerosols' indirect effects, i.e., those involving the reflectivity, lifetimes, precipitability, and coverage of clouds. The ACE investigations were organized through the International Global Atmospheric Chemistry Program (IGAC) as an approach for reducing these uncertainties. The ACE experiments preceding ACE-Asia took place in the Southwestern Pacific Ocean, South of Australia (ACE-1), in the North Atlantic Region (ACE-2), and the western Atlantic (TARFOX).

The ACE-Asia assessment of aerosol/climate relationships was designed to include anthropogenic as well as natural aerosols. The distinction between these aerosol types is not always clear, however, because

dust particles are commonly mixed with or modified by reactions with anthropogenic substances. Therefore, while the main focus of this paper is on mineral dust, we consider in some detail how these particles are modified as they mix with natural and anthropogenic substances. Indeed, determining the mixing state of the aerosol, i.e., whether the particles are internally mixed (multiple components mixed in single particles) or externally mixed (admixtures containing different types of particles) is critically important because it has major implications for the aerosols' influence on climate. As an example of this, calculations in Seinfeld et al. (2004) indicate that under cloud-free conditions, the internal mixing of organic and elemental carbon with sulfate and dust particles over Asia can result in a net change in climate forcing of > 1 W m^{-2} relative to the externally mixed case.

In preparing these summaries, the authors were asked to consider a set of questions in an attempt to integrate our discussion of the ACE-Asia dust/climate studies. The questions posed were as follows:

(1) Do we know anything more about trace elements in Asian dust than we did before the experiment?
(2) How does the dusts' size distribution change with distance from the source?
(3) How do dust concentrations vary vertically? How do ground station measurements relate to what is in the column?
(4) How does dust affect the chemistry of nitrogen and sulfur oxides?
(5) How much of the dust is modified by reactions with acids or with carbonaceous substances?
(6) What is the growth factor for dust as a function of relative humidity, and how does this change during transport?
(7) What are the dusts' radiative properties and radiative impact?
(8) What are the health effects or other biological impacts caused by dust?

3. Research strategies and operations

Several key elements of the ACE-Asia strategy for quantifying the relationships between aerosols and their climatic impacts were the efforts to (1) characterize the spatial and temporal patterns in aerosol properties, (2) determine how the aerosol composition and properties vary with altitude, and (3) intercalibrate and intercompare measurements among platforms (Huebert et al., 2003). Another important component of the strategy was to involve chemical transport modelers in the planning, execution and interpretative phases of the studies; this also included tests of consistency between models and measurements, mainly through various types of closure experiments.

Chemical transport models (CTM) were used during the field operations phase of the experiment, that is, to provide direct estimates of quantities being measured, such as the concentrations of selected aerosol species and optical thicknesses; this information was then used to develop flight plans with specific targets or objectives. Such planning is particularly useful for studies of Asian dust because the distributions of mineral aerosol over Asia and the western north Pacific are highly changeable in space and time.

With reference to scientific operations, an intensive observation period (IOP) for ACE-Asia took place from mid-March to late-April/early-May 2001 while studies at a network of ground stations were conducted over a longer period of time (see Fig. 1 for station locations). Sampling during the IOP was coordinated among aircraft, oceanographic research vessels, satellites, and the ground stations. Two of the aircraft, a Lockheed C-130A and a Twin Otter were based out of the (U.S.) Marine Corps Air Station at Iwakuni, Japan while a third, which was mainly used for studies of aerosol/cloud interactions, operated out of Kagoshima, Japan. The NOAA R/V Ronald H. Brown and the R/V Mirai of the Japan Marine Science and Technology Center were instrumented for studies of the aerosols' optical and chemical properties during the IOP.

Surface measurements were made from a network of ground stations, including super sites in Korea, China, and Japan. The most heavily instrumented of these sites was Gosan (126°10′E, 33°17′N), located on the far western edge of Jeju Island ~300 m west of the Upper Air and Radar Meteorological Site, operated by the Korea Meteorological Administration. Several intensive and routine measurement campaigns including PEM-West A and B were previously carried out at Gosan (Arimoto et al., 1996; Park et al., 2004). Some twenty different institutions from six countries sampled at Gosan during ACE-Asia (Huebert et al., 2003), and the instrumentation there included two lidars for studies of aerosol backscatter, vertical profiles and size distributions. Additional studies were conducted on Mt. Halla, the tallest mountain in South Korea, located near the center of Jeju.

A second ACE-Asia super site was located at Zhenbeitai, Shaanxi Province, People's Republic of China (38°17′N, 109°43′E). There a 20-m tall tower was used for air sampling, and the operations were led by the Institute of Earth Environment, Chinese Academy of

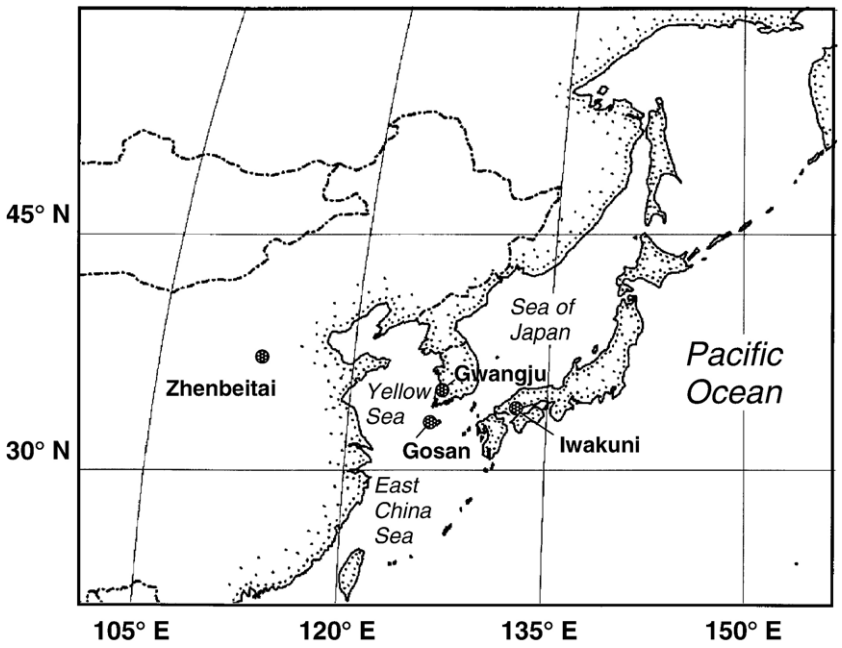

Fig. 1. Locations of ACE-Asia ground-based sampling stations at Gosan and Gwangju, Korea and Zhenbeitai, People's Republic of China. The NCAR C-130 aircraft was deployed from Marine Corps Air Station, Iwakuni, Japan.

Sciences. This site is located in a transitional zone from semi-arid to arid desert-like conditions, ~1100 m above sea level. Zhenbeitai lies on the northeastern flank of the loess plateau near the eastern margin of the Mu Us Desert, a major source for mineral dust.

4. Results and discussion

Most fortuitously, several major dust events occurred during the ACE-Asia IOP. One event, which blanketed much of eastern Asia from about April 5 to 15, 2001, was particularly noteworthy because it was one of the most severe dust storms in recent years, even being dubbed "The Perfect Dust Storm" (PDS, e.g., Holden, 2001). Numerical analysis performed with a dust-aerosol model (Liu et al., 2003a,b) showed that cyclones in Mongolia and cold fronts accompanying low pressure systems were major forces involved in the mobilization and transport of the dust. During the PDS, several research flights were conducted to measure aerosol extinction, characterize aerosol mass/particle size distributions, investigate dust/radiation gradients, perform inter-comparisons with other platforms, etc. Additional studies of dust were made from the aircraft and other platforms during a second large dust event on April 23.

Not all of the scientific questions asked of the co-authors are addressed here, but several recurring themes have emerged from the ACE-Asia studies, and these are highlighted in the summaries that follow. In particular, large quantities of aerosols are produced as a result of coal combustion and biomass burning in Asia, and these materials commonly become mixed with dust. The impact of mixing is not yet well constrained, but the bulk of the evidence is that this is likely a second-order concern. In addition to particle–particle processes, heterogeneous reactions occur on the dust particle surfaces, thus removing some potential aerosol precursors from the gas phase. Such reactions have important implications for aerosol number and size distributions and for particle composition; these in turn affect the aerosols' radiative properties, their impact on climate and their ultimate fate. The summaries also show striking variations in aerosol concentrations and properties with altitude, and they show that boundary layer measurements generally are not a good indicator of the aerosol properties above the surface.

4.1. Optical properties of atmospheric aerosols measured at ground stations in Korea and China

A summary of the optical properties of aerosols measured in the Asia Pacific region around the time of the ACE-Asia IOP is presented in Table 1. During this time three Asian dust storms reached Gwangju, a city of ~1.4 million on the southwestern tip of the Korean

Table 1
Summary of aerosol optical properties measured over the Asia/Pacific region

Site	Conditions and period	Optical depth, τ	Ångstrom exponent, α	Light absorption coefficient, σ_{ap} (Mm^{-1})	Light scattering coefficient, σ_{sp} (Mm^{-1})	Single scattering albedo, ω
Gwangju, Korea [a]	Dust 22–23 March 2001	–	–	48 (fine) 23 (coarse)	629 (fine) 323 (coarse)	0.93 (fine) 0.93 (coarse)
	Dust 10–13 April 2001	–	–	47 (fine) 15 (coarse)	472 (fine) 99 (coarse)	0.90 (fine) 0.90 (coarse)
	Dust 25–26 April 2001	–	–	63 (fine) 20 (coarse)	359 (fine) 85 (coarse)	0.85 (fine) 0.81 (coarse
Gwangju, Korea [b]	1999–2001	τ_{501}	$\alpha_{870/501}$	–	–	–
	Biomass burning	0.36±0.03	1.19±0.13	–	–	–
	Asian dust	0.57±0.13	0.33±0.12	–	–	–
	Urban pollution	0.21±0.10	1.70±0.27	–	–	–
Gosan, Korea [c]	Dust 10–13 Apr. 2001	0.74(τ_{500})	0.38($\alpha_{412/675}$)	22±11	240±64	0.91±0.03
	Pollution 21–24 Nov. 2001	0.28(τ_{500})	1.31($\alpha_{412/675}$)	25±13	244±123	0.88±0.02
Ship R/V Ron Brown [d]	Dust regions (ACE-Asia IOP)	–	–			0.92−0.96
	Polluted regions (ACE-Asia IOP)					0.90−0.94
Aircraft C-130 [e]	Dust (ACE-Asia IOP)	–	–	9±11	135±148	0.95±0.02
	Pollution (ACE-Asia IOP)	–	–	9±5	55±34	0.88±0.03
Gosan, Korea [f]	April 2001	–	–	–	–	~0.88
Anmyun, Korea [f]	April 2000	–	–	–	–	~0.86
Amami-Oshima, Japan [f]	April 2001	–	–	–	–	~0.85
Mandalgovi, Mongolia [f]	1998–2000	–	–	–	–	0.94 (500 nm)
Dunhuang, China [f]	1998–2000	–	–	–	–	0.90 (500 nm)
Yinchuan, China [f]	1997–2000	–	–	–	–	0.91 (500 nm)
Sri-Samrong, Thailand [f]	1997–2000	–	–	–	–	0.91 (500 nm)
Yulin, China [g]	30 March to 1 May 2001 Pollution period	–	–	6±9 (565 nm)	125±110 (530 nm)	0.94±0.05
	30 March to 1 May 2001 Dust period	–	–	7±12 (565 nm)	207±251 (530 nm)	0.96±0.04
Zhenbeitai, China [h]	April 2002	–	0.19±0.18	–	–	0.89±0.03 (441 nm)
		–	–	–	–	0.95±0.02 (873 nm)
Yasaka, Japan [i]	March and April 2001	–	0.50 (dust)	–	–	0.65–0.95 (550 nm)
	Dust period	–	1.40 (other)	–	–	–

[a] Kim, K.W. et al. (2004).
[b] Ogunjobi et al. (2004).
[c] As reported in Kim et al. (2005).
[d] Quinn et al. (2004).
[e] Anderson et al. (2003).
[f] Kim, D.-H. et al. (2004).
[g] Xu et al. (2004).
[h] Alfaro et al. (2003).
[i] Höller et al. (2003).

Peninsula. Kim, K.W. et al. (2004) showed that the chemical composition of aerosols at Gwangju varied with local air conditions and transport pathways. These authors also reported that the single scattering albedos (ω, the ratio of the light scattered by the aerosol to total extinction) during the three dust events at Gwangju averaged 0.93, 0.90, and 0.84: the values during the first two dust storms were considerably higher than the mean ω for non-dusty periods of 0.85.

Biomass burning products are some of the main substances that mix with Asian dust. In Northeastern Asia, agricultural wastes are commonly burned in open fields soon after harvest, and these burning operations are a major source for anthropogenic aerosols and gases. There are two main types of biomass burning in Korea: one is the burning that takes place after barley is harvested in late spring, and the other follows the harvesting of rice in fall. The high concentrations of fine particulate matter resulting from these burning activities also cause a degradation of visibility and adverse effects on air quality and human health (Ryu et al., 2004).

Lee, K.H. et al. (2004) reported that the annual concentration of $PM_{2.5}$ (i.e., particles less than or equal to 2.5 μm aerodynamic equivalent diameter) measured at Gwangju peaked in spring due to Asian dust and then decreased in summer when rains cleansed the atmosphere. The influence of biomass burning was most evident in June, October and November when the concentrations of $PM_{2.5}$ particles were comparable to those in spring (Fig. 2). Overall, biomass burning aerosols accounted for 40% to 43% of the total $PM_{2.5}$ in Gwangju. When biomass burning took place at the same time as Asian dust events, the aerosol optical depths (τ) were found to be 0.57, and 0.36, respectively; these were 70% to 170% higher compared with those during typical periods of urban pollution.

The Ångstrom exponent (α, the ratio of aerosol optical depths measured at two wavelengths, λ, in this case 501 and 870 nm) at Gwangju during Asian dust periods was 0.33 compared with 1.19 during biomass burning periods (Ogunjobi et al., 2004). As α is inversely proportional to particle size, the difference between dusty and polluted conditions can be explained by the dominance of coarse particles during dusty periods and higher proportions of fine particles during biomass burning episodes.

Studies at the Gosan super site showed that the mean ω (λ=550 nm) under polluted conditions was lower than that during a dusty period (0.88 vs. 0.91, respectively, Kim et al., 2005). These authors deduced —through comparisons of σ_{ap} (the light absorption coefficient) and ω between Yulin and Gosan—that significant amounts of light-absorbing pollutants were added to the dust plume during transport. That is, ω decreased as the air masses passed from the dust source region to Gosan due to the mixing of fine pollution particles with the mineral dust (Höller et al., 2003; Kim et al., 2005). Kim, D.H. et al. (2004) similarly found that dust particles from various areas of Korea and Japan have quite different absorption/scattering characteristics depending on the sites' latitudes, which in effect should be linked to differences in origins for the dust and mixing during transport. The hypothesis that the mixing of industrial and urban pollution with dust significantly

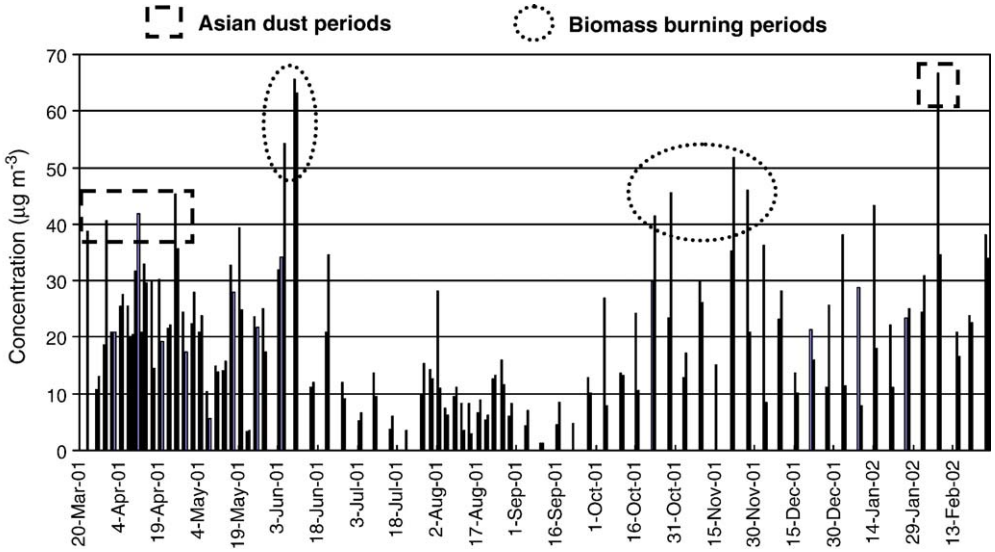

Fig. 2. Variation of $PM_{2.5}$ mass concentrations at Gwangju, Korea in 2001.

affects light absorption during dust storms is supported by chemical data as described in the next section.

With respect to the relative contributions of dust and pollution to the aerosols' radiative effects, Xu et al. (2004) compared light-scattering data for two different aerosol types at Yulin, China: local pollution dominated versus desert-dust dominated. Although the mass scattering efficiency of dust is much lower than that of aerosols from local pollution sources, the mean σ_{sp} (scattering coefficient) of the dust was still roughly 1.7 times that of local pollutants. This is because the mean $PM_{2.5}$ mass concentration of dust is about 4 times greater than that of the pollutants. This same dominant effect of dust on light scattering as a result of high mass loadings has been shown for the trade wind regime over the North Atlantic (Li et al., 1996).

4.2. Chemical composition of aerosols collected at Gosan and Mt. Halla, Korea

Park et al. (2003) presented data for the concentrations of twelve elements and eight inorganic ions in two extensive sets of spring-time, total suspended particle (TSP), samples collected at Gosan. One set of samples was collected between 1993 and 1996 for elemental analyses, with 9 and 135 daily samples collected during dust storm and non-dust storm conditions, respectively. The corresponding numbers of samples collected between 1992 and 1999 for aerosol ion studies are 16 and 445, respectively. Student's *t*-tests, based on the homogeneity of the distributions, which were verified by preliminary *F*-tests, were run to determine whether the concentrations of elements and ions differed between the dusty and non-dusty periods.

During dust storms, the concentrations of crustal elements, such as Al, Fe, Ca, and Ti, were as expected higher than in non-dust storm periods, but the concentrations of most anthropogenic elements such as Mn, V, Ni, Cu, Cd, and Cr were not statistically different (Park et al., 2003, Table 2). The only anthropogenic element showing elevated concentrations during dust storms was Pb. In addition, the concentrations of water-soluble ions such as K^+, Ca^{2+}, and Mg^{2+} were higher during dust storms, presumably due to their solubilization from mineral particles. Related studies by Arimoto et al. (2004) have shown that the concentrations of various cations (Na^+, K^+, Ca^{2+}, Mg^{2+}) in aqueous extracts of TSP filters from Gosan were well correlated with total Al, supporting an association between these water-soluble cations and dust. However, a lower percentage of soluble calcium at Gosan (~60%) compared with Zhenbeitai (~100%), suggests either a difference in the composition of the dust at the two sites or yet another effect of pollutants mixing with the dust during transport.

Table 2
Elements and aerosol ions that were found to be statistically higher/not higher during dust storm than non-dust storm periods observed at Gosan (Park et al., 2003)

	Higher	Not higher
Elements (1993 to 1996)	Al, Fe, Ca, Zn, Ti, Pb	Mn, V, Ni, Cu, Cd, Cr
Ions (1992 to 1999)	K^+, Ca^{2+}, Mg^{2+}, NO_3^-, Cl^-, SO_4^{2-}, nss-SO_4^{2-}	NH_4^+, Na^+

Of the anions with strong anthropogenic sources, the concentrations of NO_3^- and SO_4^{2-} (including non-sea salt sulfate, NSS) were higher during dust storms than under non-dusty conditions. Previously it has been observed that aerosol Ca^{2+} at Gosan is more closely related to NO_3^- than to other anthropogenic species, such NH_4^+ or SO_4^{2-} (Kim et al., 1998). Similarly, the data of Park et al. (2004) for the TSP samples from 1992 to 2002 show that the concentration of nss-Ca^{2+} was strongly correlated with NO_3^- ($r=0.63$), but the correlations were much weaker between nss-Ca^{2+} and two anthropogenic species, NSS ($r=0.34$) and NH_4^+ ($r=0.09$). Also, it has also been reported that coarse mode NO_3^- at Gosan was strongly correlated with Ca^{2+} while fine mode NO_3^- showed significant relationships with various other anthropogenic species (Kim, N.K. et al., 2004). These results can be taken as evidence that surface reactions involving nitrogen oxides—most likely HNO_3—occur on dust particles, especially those containing carbonate, during transport (Song and Carmichael, 2001; Usher et al., 2003).

An important point worth mentioning here is that the composition of dust sampled at Gosan and other surface sites may well differ from that of the dust transported long distances. This is because the effects of mixing and the reactions with pollutants are certain to be different for dust sampled near the Earth's surface compared with that transported 4 to 6 km aloft (Sun et al., 2001; Arimoto et al., 2004). In effect, some of the dust transported long distances may simply pass over plumes of pollution with little or no mixing while more extensive interactions occur between near-surface dust and anthropogenic materials. In this regard, Uematsu et al. (2002) reported that mineral dust and anthropogenic particles are sometimes transported in separate air masses to the western North Pacific, and some examples showing distinct layering of dust and pollution aerosols are presented below. We next compare data for aerosol

composition at Gosan, which sits on a cliff ~70 m above sea level (asl), with matched data from a site on Mt. Halla ~1100 m asl.

Measurements of atmospheric aerosols with a short time- and fine size-resolution are useful for comparing dust from near the Earth's surface with that aloft, and more generally for characterizing the properties, transport, and transformations of atmospheric aerosols. During the ACE-Asia IOP, 3-h time resolved and eight size-class (less than PM_{10}) resolved measurements of elemental composition were made using a DRUM sampler (Cahill et al., 1985; Raabe et al., 1988) at Gosan and Mt. Halla. The trace element composition and elemental ratios for these two sets samples were determined by X-ray fluorescence, and the results show differences in the characteristics of the air sampled at the two sites.

A comparison of the Cu/Al mass ratios indicates that local pollutants were more prevalent at Gosan than at Mt. Halla (Fig. 3). For this comparison, Al was selected as a tracer of natural dust while Cu was used to represent anthropogenic sources. Although the air transport pathways were similar at two sampling sites during the periods labeled A and C in Fig. 3, the Cu/Al ratio at Gosan was much higher than at Mt. Halla. This indicates that more anthropogenic materials were mixed with the aerosols at Gosan because the anthropogenic emissions of Cu into the atmosphere (on a global basis) exceed the dust-associated Cu flux by roughly 5- to 10-fold (Nriagu and Pacyna, 1988). Fig. 3 also compares the Cu/Al ratios at the two sites when the origins for air masses being sampled were different (period B). During that time, the air mass sampled at Gosan came from a marine region while that sampled at Mt. Halla originated from a continental region in China. But even under those conditions, the Cu/Al ratio at Gosan was higher than at Mt. Halla. This comparison illustrates some differences between surface dust versus dust aloft, and from these results one might infer that the dust sampled at the Mt. Halla site has been less modified by reactions with pollutants compared with dust from Gosan.

Further comparisons of the summary data in Table 3 show that the elemental ratios at Mt. Halla during the first Asian dust period generally were similar to those at Zhenbeitai when dusty conditions prevailed, but one element showing perplexing results is Ca. Alfaro et al. (2003) showed that the Ca/Al mass ratios in aerosols from Zhenbeitai were higher when anthropogenic emissions were dominant, possibly due to the presence of construction dusts containing CaO. Results from Gosan and Mt. Halla, however, show relatively small and inconsistent differences in Ca/Al between dusty and polluted periods (Table 3). Confounding the interpretation further are data from Chinese desert regions and the loess plateau, where the Ca/Al ratios were found to be substantially higher than at either Gosan or Mt. Halla (Zhang et al., 2001). The Ca/Al ratios reported for the desert regions and loess plateau were 1.9 and

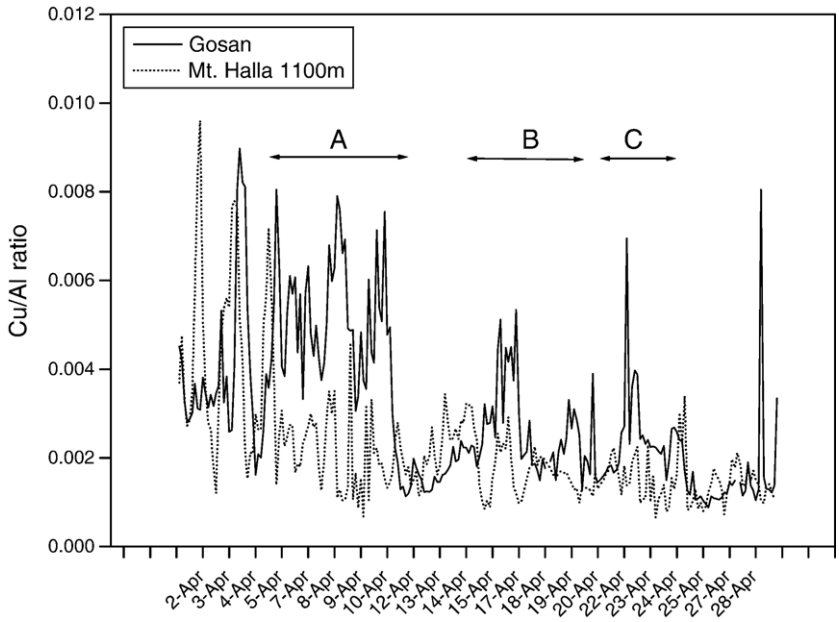

Fig. 3. Comparison of Cu/Al ratio between Gosan and Mt. Halla site during the ACE-Asia IOP. During periods A and C, the air mass pathways to the two sites were similar while those during period B were different.

Table 3
Comparison of elemental ratios for dust events observed in Northeastern Asia and other regions

Sampling site	Ca/Al	Fe/Al	K/Al	Mg/Al	Si/Al	Ti/Al	Si/Ca	Si/Fe	Fe/Ca	K/Fe	Source of data
Gosan, 11–15 April 2001	0.56	0.48	0.28		1.44	0.05	2.69	3.05	0.90	0.58	This study
Gosan, 25–26 April 2001	0.41	0.45	0.25		1.54	0.05	3.81	3.49	1.10	0.56	This study
Gosan, Clean Continental [a]	0.63	0.69	0.32		1.45	0.11	2.43	2.21	1.15	0.48	This study
Gosan, Northern China/Korea [b]	0.58	0.56	0.33		1.60	0.07	3.00	2.90	1.03	0.59	This study
Gosan, Stagnant Local [c]	0.51	0.68	0.32		1.59	0.09	3.15	2.36	1.35	0.48	This study
Mt. Halla, 11–15 April 2001	0.72	0.67	0.40		1.83	0.07	2.71	2.78	0.98	0.60	This study
Mt. Halla, 25–26 April 2001	0.51	0.58	0.33		1.95	0.08	3.84	3.34	1.15	0.56	This study
Zhenbeitai, China (Dust)	0.79	0.63	0.31	0.32	2.79	0.05	3.53	4.43	0.80	0.49	Alfaro et al. (2003)
Zhenbeitai, China (Pollution)	1.14	0.64	0.37	0.33	2.83	0.06	2.48	4.42	0.56	0.58	Alfaro et al. (2003)
Zhenbeitai	1.0	0.59	0.32	0.35	1.9	–	(1.7) [d]	(3.5)	(0.48)	(0.60)	Arimoto et al. (2004)
RV/ Ronald H. Brown		0.57		0.33							Bates et al. (2004)
Chinese Desert Regions	1.9	0.82	0.47		3.9	0.12	–	–	–	–	Zhang et al. (1998)
Loess Plateau	2.7	0.77	0.95		2.5	0.14	–	–	–	–	Zhang et al. (1993)
Tibetan Plateau	0.91	0.61	0.28		4.6	0.06	–	–	–	–	Zhang et al. (2001)
Average Crustal Material	0.37	0.43	0.34		3.83	0.04	10.27	8.80	1.17		Taylor and McLennan (1995)
African Dust (Barbados)	0.29	0.51	–	0.37	–	–	–	–	(1.76)	–	Arimoto et al. (1995)
African Dust (Eastern US)	0.15	0.47	–		1.84	–	12.2	3.84	3.19	–	Perry et al. (1997)
African Dust (Puerto Rico)	(0.38)	(0.30)	(0.17)	(0.12)	2.12	(0.05)	5.55	7.14	(0.78)	(0.59)	Reid et al. (2003)

[a] 26 March–2 April, 15–16 April, clean conditions perturbed by continental aerosols.
[b] 3–4, 21–23, 27 April, flow from northwestern China/Korea, a mixture of continental and regional aerosols.
[c] 9–10 April 2001, stagnant local, hazy conditions impacted by local pollution.
[d] values in parentheses were calculated from ratios presented in the original references.

2.7, respectively, and these were not only higher than the ratios for dust storm samples from Gosan and Mt. Halla but also higher than the polluted samples from Zhenbeitai.

The situation regarding Ca is interesting and worth pursuing because further comparisons of the data in Table 3 show large differences between the Ca/Al, Si/Ca, and Fe/Ca ratios for Asian dust versus African dust. For example, data in Perry et al. (1997) indicate that the Ca/Al ratio for African dust sampled in North America was 0.15 while Arimoto et al. reported a Ca/Al ratios of 0.29 for African dust at Barbados, 0.33 at Bermuda and 0.36 at Izaña. As shown in Table 3, these African dust ratios are much lower than those for Asian dust (0.41 to 0.79).

In related studies, VanCuren and Cahill (2002) argued that Al/Ca and K/Fe ratios could be used to chemically distinguish Asian from African dust. The Asian dust samples they collected in North America had Ca/Al ratios above 0.38 (these were actually reported as Al/Ca ratios below 2.6) while the Al/Ca marker they used for African dust was < 0.26 based on the study of Perry et al. cited above. In addition, the K/Fe ratios for the Asian dust were consistently above 0.5 while the ratios for African dust tended to be lower. These differences in the K/Fe ratios presumably reflect differences in the composition of the dust, but they also may confounded by contributions from biomass burning products. For example, Lawson and Winchester (1979) showed many years ago, and this has been repeatedly confirmed (e.g., Andreae, 1983), that K is often enriched in aerosols over soil or crustal values as a result of biomass burning.

4.3. R/V Ronald H. Brown dust studies

The dominant result of the measurements made onboard R/V *Ronald H. Brown* (RHB) during ACE-Asia was the pervasive impact of dust on the chemical composition, size distribution, and optical properties of the aerosol. Unlike previous regional experiments (ACE 1, Aerosols99, ACE 2, and INDOEX), dust dominated the mass of the super-micrometer (super-μm) and sub-10 μm size fractions and made a significant contribution to mass in the sub-micrometer (sub-μm) size range as well. As a result, mineral aerosol particles often dominated the super-μm and sub-10 μm light scattering.

RHB first encountered significant levels of dust on April 10 when a passing front brought dust-laden air down to the surface. The volume/size distribution showed an initial peak of coarse-mode (dust) aerosol followed by a peak of "pre-frontal" accumulation-mode aerosol, and finally a return to the dust-dominated coarse-mode aerosol (Bates et al., 2004). The ship encountered two additional peaks of dust-dominated aerosol on April 12 and 13. On April 12, a broad high-

pressure ridge was situated over western Asia, and the northwesterly winds associated with this system crossed arid regions of China, the Yellow Sea, and Korea before arriving at the ship. Back trajectories show that the air mass sampled during that period passed over arid regions of China, went offshore near Shanghai and changed direction when it encountered a transient anticyclone near 124°E. The CFORS chemical transport model (Uno et al., 2003) clearly captured the major pulses of dust shown in Fig. 4 that reached the surface along the ship's track.

The passage of the front on April 10 brought elevated concentrations of sub-μm and super-μm dust to the ship. The sub-10 μm dust concentrations measured on the ship reached 140 μg m^{-3} on April 12; this was about one-third of the concentrations measured at Zhenbeitai by Zhang et al. (2003a,b) during this same period. From April 10 to 14, dust composed 8% to 31% of the sub-μm mass and up to 80% of the super-μm mass. Hence, at no time was "pure" dust measured on the ship. Rather, the dust was invariably mixed with pollutant aerosols that came from a variety of source regions, and these varied with the transport pathway to the ship.

Chemical analyses of RHB samples show that the measured average Fe/Al (0.58 ± 0.07) and Mg/Al (0.33 ± 0.07) ratios (Table 3) were consistent with a dust source located in the "northern high desert" (Alfaro et al., 2003). The super-μm dust-laden aerosol also contained sulfate and nitrate. The Cl^-/Na^+ ratio increased during the high dust period, suggesting that sulfate, and in particular nitrate was less associated with the sea salt aerosol and more associated with the higher-buffering-capacity desert dust. Data obtained with an Aerosol Time of Flight Mass Spectrometer (ATOFMS, see below) are particularly revealing because they show that the nitrate and dust particles often were internally mixed. In addition, variable NO_3^-/Al mass ratios suggest that most of the nitrate was a result of secondary aerosol formation. Super-μm sulfate behaved in a manner similar to NO_3^-, being associated with sea salt in the pre-frontal air and with dust in the post-frontal air. These results add to the growing evidence (see review by Usher et al., 2003) that sorption and oxidation of trace gases on dust particles is an important pathway for sulfate and nitrate formation.

During the April 10 to 14 dust period, the highest sub-10 μm scattering coefficients of the experiment

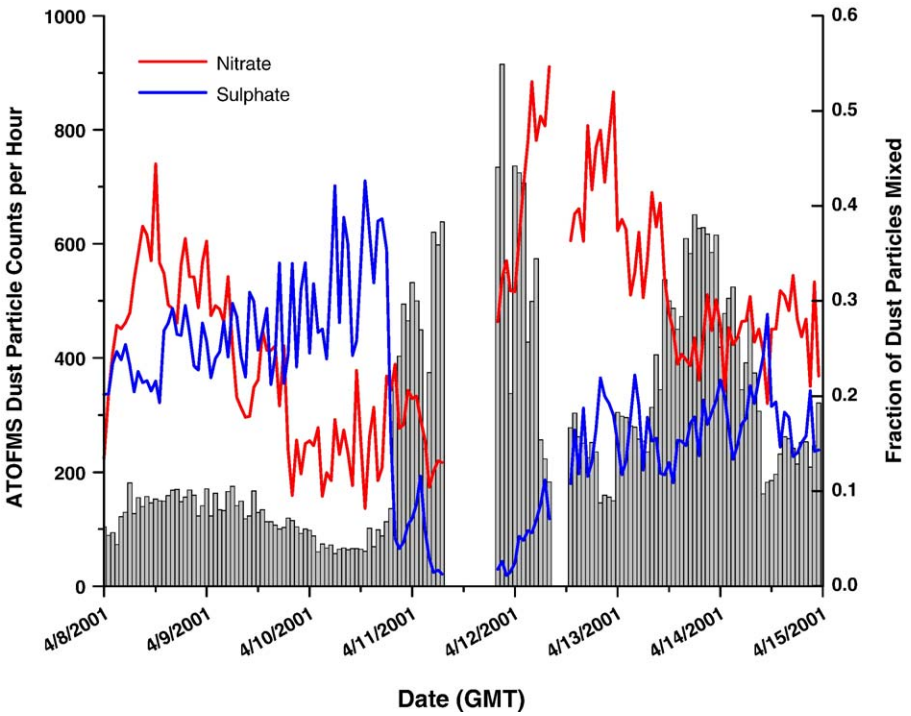

Fig. 4. Total dust particle counts (bars) and estimates of the fraction of dust that was mixed with nitrate or sulfate (lines) from ATOFMS measurements. Dust particles with peak areas > 5000 for NO_3^- (m/z −62) or HSO_4^- (m/z −97) are considered mixed. The ATOFMS dust particle counts have not been scaled to the total atmospheric concentrations.

were measured, with values up to 330 Mm^{-1} reported (RH = 55% and λ = 550 nm, Quinn et al., 2004). The fine fraction of scattering (sub-1 μm scattering/sub-10 μm scattering) was low relative to measurements of polluted air masses during ACE-Asia, with a mean value around 0.5 ± 2.

The average sub-10 μm light absorption coefficient for the dusty periods was 12.1 ± 6.4 Mm^{-1}. Mean values of the fine fraction of absorption during these same periods ranged from 73% to 77% indicating that, on average, 23% to 27% of the sub-10 μm absorption was due to super-μm particles. The fine fraction of absorption was higher during the dust period compared with the pollution episodes. Images of individual particles indicate the presence of several kinds of super-μm soot, including dust–soot aggregates and solitary black carbon cenospheres (formed by pyrolysis during combustion of heavy fuel oil or coal), which contributed to super-μm absorption (Quinn et al., 2004). During dusty periods, the median percentage of EC in the super-μm size range was 42 ± 15% compared to 13 ± 13% during the non-dusty periods. The median percent of super-μm absorption during dusty periods was 21 ± 12% compared to 8 ± 6.7% for non-dusty periods. Total non-sea salt, non-crustal K^+ also was elevated in these samples suggesting a biomass/biofuel source contribution (Bates et al., 2004).

The super-μm absorption was overwhelmed by super-μm scattering in dusty air, however, resulting in relatively high values for ω. The mean, ambient RH, super-μm, ω for the dust regions ranged between 0.97 and 0.99. Hence, the super-μm soot appears to have had a negligible effect on the super-μm ω (Quinn et al., 2004). The larger implication for the soot–dust aggregates is that the atmospheric lifetime of soot will be shortened due to its association with super-μm particles that rapidly deposit.

During the dusty period, the aerosol's hygroscopic growth was substantially suppressed when compared to other periods (Carrico et al., 2003). This was particularly the case for sub-10 μm aerosol but also true for sub-1 μm aerosol with representative values for the hygroscopic growth factor at 82% relative humidity (the ratio of scattering at 82% relative humidity, RH, to scattering at low RH, $f_{RH=82\%}$) of 1.69 ± 0.25 and 2.10 ± 0.29, respectively. For the most dust-dominated period (April 11 to 12), when 90% of the super-μm mass and 50% of the sub-μm mass was dust, the aerosol was nearly hydrophobic with $f_{RH=82\%}$ of 1.18 and 1.39 for the sub-10 μm and sub-1 μm aerosol, respectively. Despite the low hygrosopicity, the dust-influenced aerosol showed strong deliquescence, crystallization, and hysteretic properties. On average, the deliquescence humidity and the crystallization humidity values for the dust aerosol were 79 ± 1% and 43 ± 2%, respectively. The hygroscopic behavior during dusty periods most likely reflects a mixture of a nearly non-hygroscopic dust aerosol with a secondary contribution of more hygroscopic sea salt and pollution aerosol.

The measurement approach taken on the RHB (i.e., the collection of an over-determined data set) revealed many challenges for measurement and modeling techniques employed even though they were state-of-the-art. Comparisons between measured and calculated aerosol mass and scattering yielded agreement within the overall experimental uncertainty. However, this agreement was not definitive because the comparisons relied on assumptions regarding particle shapes that were not extensively tested by measurements. In addition, the scattering closure study required assumptions about the response of sizing instruments (differential mobility particle sizers and aerosol particle sizer spectrometers) to non-spherical dust particles that have not been verified empirically. In contrast to the aerosol mass and scattering results, a comparison of measured and calculated absorption coefficients revealed systematic differences. For the sub-μm particle-size range, the measured absorption values were higher than the calculated ones while the opposite was true for the super-μm particles. Estimates of the contributions of various sources of uncertainty for the calculated scattering and absorption coefficients have been tabulated in Quinn et al. (2004).

Results from the RHB show two particular challenges presented by the ACE-Asia aerosol (1) the nonsphericity of the particles and (2) mixing state of the dust aerosol (that is, how do sizing and optical instruments respond to these factors and how are they best parameterized in optical models?). These challenges and uncertainties will require further intensive regional experiments that emphasize the collection of overdetermined data sets, instrument characterization, and instrument and model comparisons.

4.4. Aerosol-time-of-flight mass spectrometer (ATOFMS) studies on R/V Ronald H. Brown

4.4.1. General description/experimental

Measurements of the size and chemical composition of individual aerosol particles sampled from the RHB were carried out employing a transportable ATOFMS. Aerosol particles were sampled 18 m above the sea surface through a heated mast extending 5 m above the container housing the instrument. As

described elsewhere (Prather et al., 1994; Noble and Prather, 1996; Gard et al., 1997), the ATOFMS allows for characterization of the aerodynamic diameter and chemical composition of individual particles from a polydisperse aerosol. ATOFMS couples aerodynamic particle sizing with time-of-flight mass spectrometry in a single instrument, providing both positive and negative ion mass spectra for each detected particle. Distinct size-composition relationships can be derived from the acquired data, and differences in the degree of external or internal mixing within an aerosol particle population can be inferred. Generic spectral characteristics of the sea salt and dust particles observed during the campaign are described in Guazzotti et al. (2001).

The ATOFMS data are analyzed using a variety of tools. Using a Matlab™-based database, particles are assigned into exclusive classes by searching for ions of interest with specific threshold values (ion area, relative ion area, mass/charge ratios, etc., e.g., Gard et al., 1998; Silva et al., 1999; Liu et al., 2000; Angelino et al., 2001; Guazzotti et al., 2001). For example, the presence of nitrate in sea salt or dust particles can be inferred from signals at the following characteristic mass-to-charge (m/z) ratios: −46 $[NO_2]^-$, −62 $[NO_3]^-$, +30 $[NO]^+$, or +108 $[Na_2NO_3]^+$. Similarly, sulfate is identified by peaks at m/z −97 $[HSO_4]^-$, −80 $[SO_3]^-$, −96 $[SO_4]^{2-}$, or +165 $[Na_3SO_4]^+$. Also, automatic sorting and classification of particles with similar spectral characteristics is achieved using an adaptive resonance theory-based neural network algorithm, (e.g., Carpenter et al., 1991; Xie et al., 1994; Hopke and Song, 1997, Song et al., 1999). This algorithm assigns particles into chemically similar classes and generates a new class whenever a particle's mass spectrum falls outside a preset proximity relative to all existing classes.

4.4.2. Key findings

The associations of dust particles with chlorine, nitrate, and sulfate were evaluated from the ATOFMS data for single particles sampled from the RHB; these include spectral signatures and elemental ratios. Results for post-frontal periods show compelling evidence for the uptake and/or formation of nitrate and sulfate on dust particles, with as much as 60% to 80% of the super-μm nitrate and sulfate being associated with mineral particles (Bates et al., 2004; Tang et al., 2004a,b). In contrast, in pre-frontal air, 50% to 60% of the super-μm nitrate and sulfate was associated with atmospheric sea salt. These results indicate that mineral dust particles provide surface sites where scavenging and heterogeneous reactions can occur, leading to the uptake or formation of sulfate and nitrate. The association of dust particles with chlorine (m/z=−35 and −37) was evaluated as well, and in this case, detailed analysis allowed for differentiation between the presence of chlorine in dust particles due to uptake of chlorine-containing species versus coagulation between sea salt and dust particles (Sullivan et al., in press).

Unique information on the associations between the dust particles and various indicator elements can be inferred from the single-particle mass-spectral data. Most notably, the ATOFMS data demonstrate that the chemical composition of the dust particles either affects the uptake of secondary species (nitrate, sulfate, chloride) or influences reactions among acidic species. From April 10 to 16, 2001 (DOY 100 to 106), i.e., during the so-called PDS, the chloride, nitrate and sulfate ion intensities were all well correlated for dust particles having a large Ca^{2+} ion signal. In contrast, dust particles with a large Al^+ ion signal showed strong anti-correlations with these secondary species for significant parts of the PDS. In fact, the anion signals for the Al^+ containing particles varied during the event: the nitrate signal was stronger than that for chloride until April 12 when the latter suddenly became dominant. From April 14 to 15, the two anion signals were strongly correlated, but they diverged again from April 15 to 16 when the nitrate signal began to increase and chloride decreased. Parallel trends were observed when the nitrate and sulfate ion intensities for the high-Al dust particles were compared, that is, the relative strength of the nitrate signal increased compared to sulfate during the same periods described above.

The observed trends in ion signals indicate that the uptake of reactive gas-phase species may be influenced by an individual dust particle's mineralogy, as has been suggested by Krueger et al. (2004) based on laboratory studies. Interestingly, the peak-area ratios for stable elemental markers such as the Na/Al and K/Al ratios also changed when the intensities of the secondary species ion changed, and this may indicate that the source region and/or chemical weathering of the dust particles varied in relation to the air mass trajectories that reached the RHB.

Changes in the air masses' chemical composition and source regions are one possible explanation for the variations in the fractions of dust mixed with sulfate versus nitrate shown in Fig. 4. Measurements onboard the RHB showed SO_2 (g) varied between 0.5 to 2.5 ppbv, indicating that some sulfate precursor was always present in the sampled air. Unfortunately no measurements of NO_x or NO_y were made aboard the RHB so information on the availability of aerosol–nitrate precursors can only be inferred from the aerosol

composition measurements. If the dust plume passed through regions polluted with differing concentrations of precursor SO_x and NO_x species, differences in the relative amounts of sulfate and nitrate taken up may have occured, and while we cannot discount this possibility, there is evidence that competitive surface reactions on the surface of the dust particles were involved. More details on the air mass back-trajectories reaching the RHB and how these changed the bulk aerosol composition are available in references such as Quinn et al. (2004).

The ATOFMS data are particularly revealing because they can be used to estimate the fraction of reacted dust particles (Fig. 4). Here, we operationally define particles with peak areas greater than 5000 units of nitrate or sulfate markers as reacted. While this may be considered a semi-quantitative measure, methods are being developed to quantify the amount of nitrate or sulfate corresponding to the measured peak area. More to the point, it is already clear from studies of source soils that a peak area greater than 5000 units definitely represents only those dust particles that have undergone heterogeneous processing. In fact, this represents a high ion signal, and thus will most likely represent a conservative estimate of the fraction of particles that have undergone reactions. To eliminate biomass particles which can be incorrectly placed in the dust particle clusters by the neural network algorithm (ART-2a), we restricted this analysis to dust particles with a peak area of $m/z+27$ $[Al]^+>5000$. Aluminum is the best single ion marker for dust particles, and while $m/z+27$ can also be present as organic species in biomass particles, the intensity is never above this threshold (based on ambient observations as well as biomass source studies performed at the University of California, San Diego).

During the PDS, dust particles with high amounts of nitrate were more common than those rich in sulfate (Fig. 4), but both compounds were consistently present on the dust. The relative amounts of the two anions reversed around noon (Coordinated Universal Time) on April 9 when sulfate-dominant dust particle counts became the majority until about 6 pm on April 10 when nitrate again dominated. A similar but brief cross-over occurred around 10 pm on April 14. Both of these reversals occurred when the total dust particle counts decreased. A total of 41,178 dust particles, each with a peak area of $+27$ $[Al]^+>5000$ were analyzed between April 8 and 15. Of these particles 17,646 had a peak area of $m/z-62$ or $-97>5000$, the indicators for nitrate and sulfate, respectively.

These analyses produced an original and compelling result: less than 1.2% of all these dust particles had peak areas of both $m/z-62$ and $-97>5000$, and therefore, the dust particles rarely contained large amounts of both nitrate and sulfate, but rather one ion or the other. Using these procedures, we estimate that the percentage of reacted dust (per hour) varied from 13% to 67% of the total dust, with an average of 46% reacted.

Further evidence for the competitive uptake or volatilization of reactive acids by the mineral dust is presented in the form of a ternary plot of the ion markers for three major secondary particulate products, Cl^-, NO_3^-, and SO_4^{-2} (Fig. 5). The dust particles plotted are those that contain an aluminum peak area > 5000 (to exclude biomass particles, as above) and peak areas of nitrate, sulfate or chloride > 5000 between April 9 and 10 (DOY 99 and 100). To exclude any contribution from dust mixed with sea salt particles, dust particles with a peak area of m/z $+81$ $[Na_2^{35}Cl]^+>100$ also were excluded (this amounts to ~25% of the particles). A peak at $m/z+81$ is an excellent marker for sea salt and particles that have become mixed with sea salt (Gard et al., 1998; Guazzotti et al., 2001).

Competitive uptake or reactions among species (e.g. NO_x, NO_y, SO_x, ClO_x, HNO_3, H_2SO_4, HCl) leading to the formation of secondary products (Hanisch and Crowley, 2001; Usher et al., 2003; Wurzler et al., 2000) is demonstrated by the lack of particles that have m/z markers for both sulfate and nitrate or sulfate and chloride. Particles of this type would appear between the 100% HSO_4^- vertex and the 100% NO_3^- or 100% Cl^- vertex. Fig. 5 clearly shows a lack of significant numbers of particles in these areas, indicating competitive uptake and/or reactions among the various mineral acids. The dust particles used to generate Fig. 5 were measured on one day when the air mass trajectory had not changed significantly. This indicates that all the acid precursors were available to varying degrees but despite this the single dust particles did not take up both sulfate and nitrate or chloride. The competitive nature of uptake is further supported by the scatter plots shown to the left (Cl^- vs. HSO_4^-) and right (HSO_4^- vs. NO_3^-) of the ternary plot in Fig. 5. These figures further confirm that single dust particles with a large amount of sulfate typically do not also contain large amounts of either chloride or nitrate. That the production of these secondary species appears to be a competitive or exclusionary process has not been previously demonstrated for ambient mineral dust particles to our knowledge (see also Sullivan et al., in press).

Interestingly, this competition does not exist for the accumulation of nitrate and chloride. The ternary plot demonstrates that large numbers of particles contain appreciable amounts of both nitrate and chloride, that is, points lying between the 100% NO_3^- and 100% Cl^-

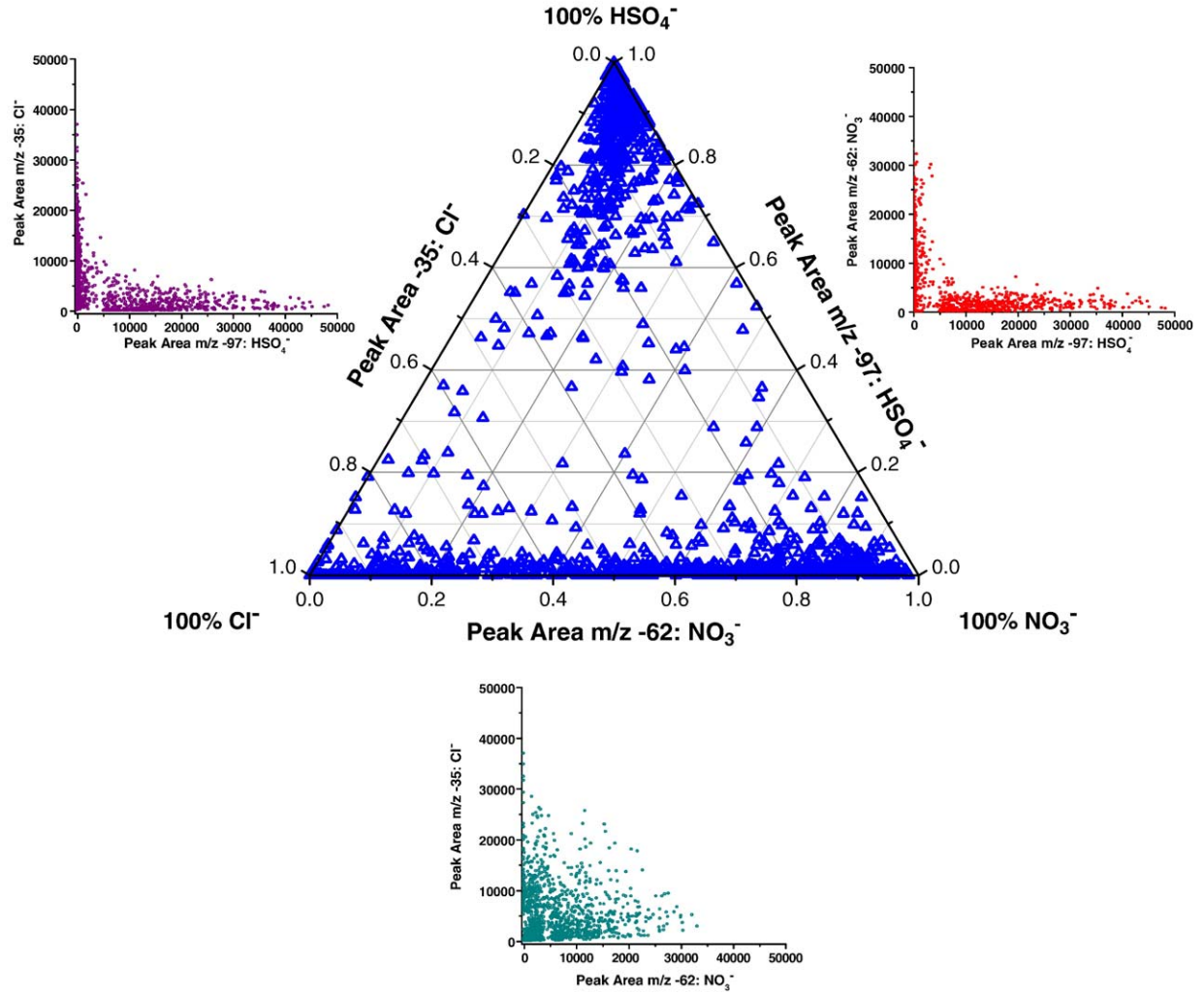

Fig. 5. Ternary plot (center) of the relative peak areas of major secondary species, nitrate, chloride and sulfate, for all dust particles analyzed by ATOFMS between April 9th and 10th that are considered mixed, excluding those mixed with sea salt or biomass particles. Each open circle represents one dust particle, 1359 in total are displayed. Each labeled vertex is the point at which the peak area for that species comprises 100% of the combined peak area for the three secondary products. Scatter plots (surrounding) are the absolute peak areas of the two secondary species for the neighboring axis of the ternary plot for the same set of particles.

vertices. The scatter plot of Cl^- vs. NO_3^- (bottom) confirms this; many particles lie towards the center of the Cl^- –NO_3^- axis, indicating significant amounts of both chloride and nitrate in the same particle. There are also fewer particles containing large peaks for just nitrate or chloride compared to the other two scatter plots (top left and right) which show particles with larger peak areas for individual acids.

The mechanism that results in the competitive behavior merits further investigation, and laboratory studies will likely be especially revealing. One possible explanation for the apparent strong competition for sulfate accumulation may lie in the low volatility of sulfuric acid (Sullivan et al., in press). In comparison, both nitric and hydrochloric acid are much more volatile, and they may displace one and other from the particle phase into the gas phase, in a manner analogous to the displacement of chloride as $HCl_{(g)}$ by HNO_3 in sea salt aerosols (Gard et al., 1998).

4.5. Radiative properties of Asian dust deduced from airborne optical measurements

4.5.1. Measured properties

During the spring of 2001, the NCAR C-130 aircraft was used to characterize the nature and variability of

dust and pollution aerosols in Asian outflow using a variety of physical, chemical, and optical techniques. The range of the aircraft and its ability to resolve vertical aerosol structure made it an essential platform for extending surface measurements. Dust size distributions were obtained optically and found to have volume-median diameters varying from a few micrometers up to over 10 μm depending upon the location, altitude and the event. Dust size distributions were found to be best represented by three lognormal modes with volume-median diameters of about 1.1, 5.5, and 14 μm (with geometric standard deviations of 1.46, 1.85 and 1.50 μm), respectively. (The diameter of the largest mode was set to the value reported by Alfaro et al. (1998); this gave a reasonable fit to the uncertain measurements of very large particles on the C-130.) These dust modes were separable from an accumulation mode aerosol typically centered near 0.3 μm that contained 5% to 15% black carbon (BC) internally mixed with other components (Clarke et al., 2004). Measured optically effective volume distributions up to 10 μm diameter are shown in Fig. 6 and reveal the mean and median distributions for dust measured for both boundary layer (below 2 km) and free-tropospheric (above 3 km) samples. These are shown for cases when the measured coarse-particle light scattering exceeded 35 Mm^{-1} in order to reduce the impact of low-dust cases upon the averages.

The light scattering and absorbing properties of the fine-mode and coarse-mode constituents were discriminated using size-segregation at a low-RH aerodynamic diameter of 1 μm, as described by Anderson et al. (2003). Measurements from 300 level-legs acquired over 19 flights were analyzed. Samples were taken to be

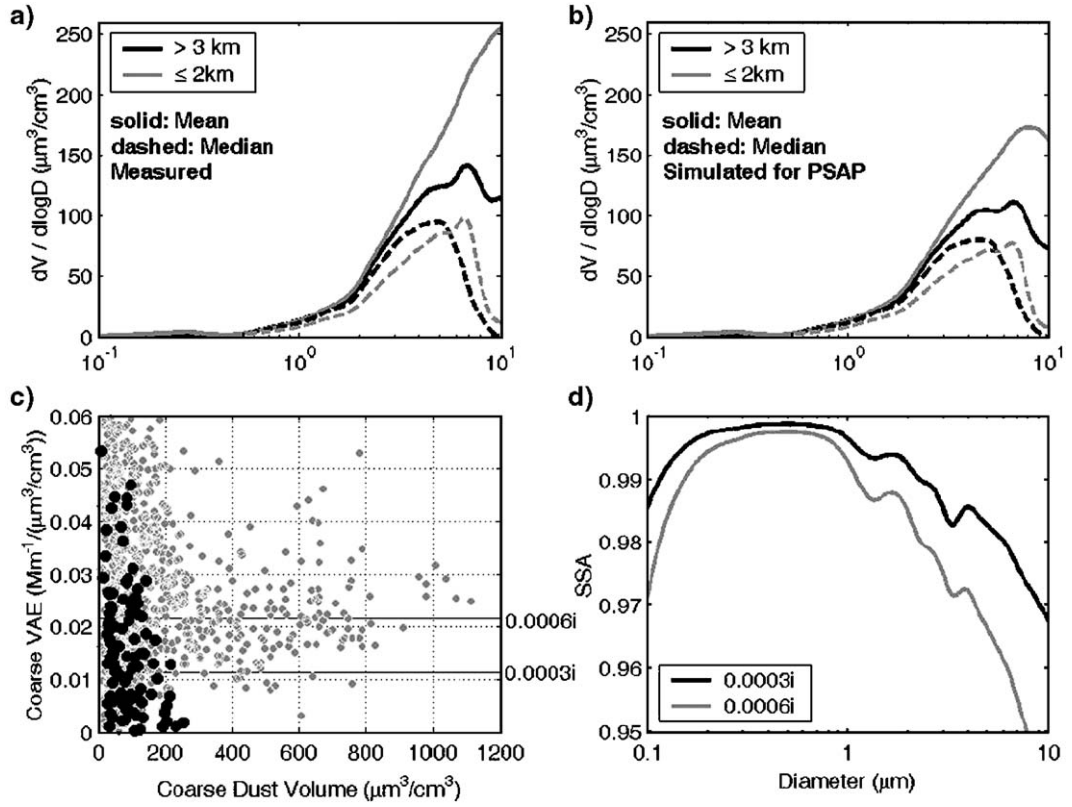

Fig. 6. Optically effective (OE) volume distributions are shown as measured with the optical particle counter (OPC) averaged over all horizontal legs below 2 km and above 3 km (a). The same distribution as expected to be passed through the Particle Soot/Absorption Photometer (PSAP) (b) for comparison with measured light absorption. The difference in mean and median shapes provides evidence for larger particles in stronger less frequent events. Particle losses are present above about 5 μm and actual ambient distributions are expected to have larger volumes than indicated for these sizes but this will have little influence on the optical analysis here. In panel (c) the coarse volume absorption efficiency (VAE) is plotted against coarse dust volume and is calculated from coarse PSAP absorption divided by coarse volume for sizes larger than 1-um aerodynamic diameter (about 0.75 μm OE diameter). Low altitude dust asymptotes to a VAE that constrains the dust complex refractive index to about 0.0006 while high altitude dust shows lower VAE values more consistent with an index near 0.0003, or lower. These refractive indices imply different size-resolved single scattering albedo values for the high and low altitude dusts (d) suggestive of different mineralogy.

dust-dominated when (a) the super-μm aerosol was responsible for 70% or more of the low-RH light scattering at 550 nm and (b) the presence of substantial sea salt could be ruled out based on the flight level and/or chemical data. The optical properties of dust were then determined as the properties of the super-μm aerosol during these dust-dominated events. Key properties determined in this way were ω (at 550 nm and low RH), $f_{RH=85\%}$, b (hemispheric backscatter fraction at 550 nm and low RH — a measure of the scattering phase function), and S (ratio of extinction to 180° backscattering — also known as the lidar ratio — at 532 nm and low RH).

Diagnostic tests were performed during the flights, and the data were combined with previous laboratory and theoretical studies to determine the 95% confidence uncertainty of each measured parameter. In addition, during ACE-Asia the C-130 was equipped with a new, low-turbulence, inlet (Huebert et al., 2004) designed to allow efficient sampling of coarse-mode dust. Closure tests with remote measurements of aerosol extinction by airborne sun photometry (Redemann et al., 2003) and by ground-based lidar (Murayama et al., 2003) indicated that in situ sampling of coarse-mode dust by this new inlet was sufficient to accurately determine its radiative properties at mid-visible wavelengths.

Light scattering and absorption by the sub-μm aerosol showed very little correlation with light scattering and absorption by the super-μm aerosol. (Coefficients of determination, r^2, were about 0.1). This finding tends to confirm the conceptual model underlying the in situ measurements — namely, that the "coarse mode" and the "fine mode" are, for the most part, independent atmospheric phenomena that can be effectively separated using a cut point of 1 μm aerodynamic diameter at low RH. Nevertheless, the two modes do interact, as revealed by chemical measurements discussed herein, and the separation at 1 μm is not perfect, as shown by size distribution measurements (Clarke et al., 2004).

Coarse-mode dust was found to have low absorption per unit mass resulting in a high ω (0.96 ± 0.01; mean and 95% confidence uncertainty)[1] and to be virtually non-hygroscopic ($f_{RH}=1.06\pm0.10$). In contrast, pollution aerosol was found to have much higher absorption per unit mass ($\omega=0.88\pm0.03$) and to be much more hygroscopic ($f_{RH}=1.73\pm0.24$). As discussed by Doherty et al. (2005), these general findings are in good agreement with surface measurements from the R/V Ron Brown and the Gosan surface site, with one exception. Coarse-mode aerosol measured at Gosan during dust events and during collocated, fly-by sampling was found to be much more hygroscopic than on the C-130. Whether this discrepancy arises primarily from instrumental or sampling differences is not known. Shipboard measurements on the Ron Brown indicated f_{RH} for dust-dominated mixed aerosol to be 1.25 (Carrico et al., 2003, see also Section 4.3, above), similar to the C-130 measurements.

We recognize that the contamination of super-μm dust by pollution could conceivably affect the derived optical properties. The addition of BC would lower ω while addition of soluble species would raise hygroscopicity. Thus, the true value of ω for pure dust might be somewhat higher and the true value of f_{RH} somewhat lower than the values reported above, but as discussed below, both these effects are thought to be small.

In terms of the scattering phase function, the properties of dust and pollution were found to be quite similar. Therefore, these values determined for dust are not sensitive to contamination by pollution. The hemispheric backscatter fraction, b, was measured as 0.12 ± 0.02 for dust and 0.14 ± 0.02 for pollution. The lidar ratio, S, was measured as 46 ± 8 for dust and 50 ± 5 for pollution. The measured lidar ratio for dust is consistent with independent measurements by raman lidar (Murayama et al., 2003).

4.5.2. Vertical distribution

The vertical variation of optical properties, averaged over all 19 flights and separated into sub- and super-μm contributions, is shown in Fig. 7. Distinct differences are evident between the boundary layer (BL; below ~2000 m) and the free troposphere (FT). Pollution — as indicated by sub-μm scattering and absorption (Fig. 7a and b, respectively) — is largely confined to the BL, while dust — indicated by coarse-mode scattering — is distributed much more evenly throughout the column. (Note that some of the super-μm aerosol in the BL is likely associated with pollution, Shi et al., 2003) As a result, the sub-μm fraction of scattering (SMF, Fig. 7c) decreases with height and is distinctly lower in the FT. For the total aerosol, ω increases and f_{RH} decreases with height (Fig. 7d and e).

These variations are seen to be primarily due to the different vertical distributions of dust and pollution. It is noteworthy, however, that ω for the super-μm aerosol increases with height, indicating a possible change in dust composition, as discussed below. We note that the observed increase in ω with height is in marked contrast

[1] Using the same absorption measurements and a methodology that incorporated measured size distributions, Clarke et al. (2004) derived an ω value for the pure dust component of 0.97 ± 0.01.

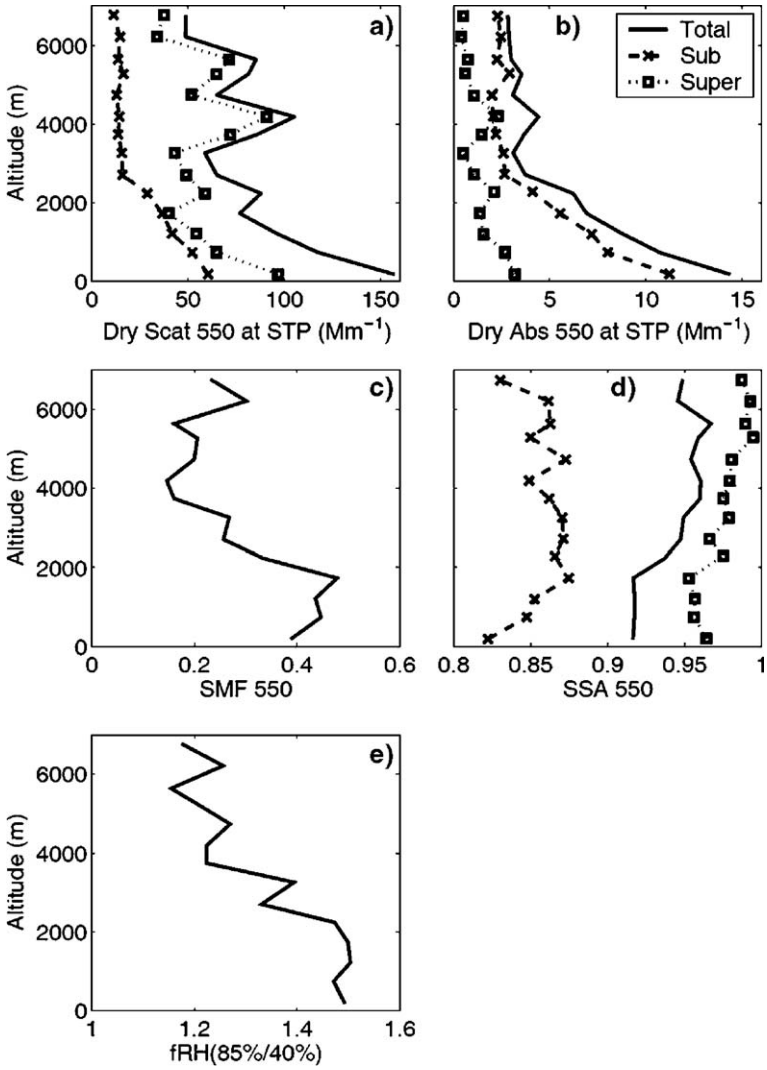

Fig. 7. Vertical variation of optical properties. Dry Scattering (a) and Dry Absorption (b) values are reported with respect to standard temperature and pressure (1013.2 mb and 273.2 K). (Scattering and absorption profiles shown in (Clarke et al., 2004; Fig. 1 therein) were reported at ambient air density, which accounts for the differences aloft.) Data have been averaged over 500 m altitude bins. For intensive properties [sub-micrometer fraction, SMF (c); single scatter albedo, SSA (c) and hygroscopicity, f_{RH} at 85% vs. 40% relative humidity (d)], extinction-weighted averages were used.

to observations made south of 25°N near southeast Asia where ω tended to decrease with height due to the increasing prevalence of biomass burning aerosol (Clarke et al., 2004).

Average ionic concentrations from the Total Aerosol Sampler (Kline et al., 2004) provide further insight into the FT/BL contrast. The median concentration of soluble Ca (an indicator of dust) above 2500 m was 2.5 μg m^{-3}, 50% greater than that in the BL below 500 m. By contrast, the ions associated with air pollution (NSS, nitrate, and ammonium) were all 3–4 times more concentrated in the BL. This had predictable effects on the molar ratios in FT dusty air. The nitrate/Ca ratio dropped from a median of 1.6 in the BL to 0.2 in the FT. Similarly, NSS/Ca ratio dropped from 1.4 in the BL to 0.3 in the FT.

The presence of dust in the FT appeared to impact the size distribution of NSS, as measured using multi-stage impactors. In the BL only 10% of NSS was on super-μm particles, but that rose to 35% in the FT. Nitrate, on the other hand, was found predominantly on super-μm particles in both the BL (89%) and the FT (78%). Indeed, the size distribution of nitrate was generally very similar to that of soluble Ca.

This altitude contrast was also evident in the optical properties of coarse-mode particles. As shown in Fig. 7d, the mean ω for super-μm aerosol is ~0.95 in the BL but ~0.99 in the FT. This result can be investigated further by returning to Fig. 6c, which shows the ratio of measured absorption to measured aerosol volume — a quantity we denote as the volume absorption efficiency (VAE, see Clarke et al., 2004). Because laboratory tests revealed that the absorption-measuring device did not effectively sample the largest particles, we define VAE with respect to volume distribution actually sampled. Data on VAE from differential total and sub-μm absorption measurements is seen to be very noisy, especially at low dust concentrations. However, it is clear that the FT aerosol has values substantially and systematically lower than the BL aerosol. The solid horizontal lines in Fig. 6c denote values of imaginary refractive index appropriate to each of these cases: 0.0006 in the case of the BL dust and 0.0003 for the FT dust. These values are used to generate the plots (Fig. 6d) of size-dependent ω consistent with dust at these two altitudes. The differences uncovered by this analysis suggest that the FT and BL dust may have been systematically different in terms of mineralogy and hence either affected by sorting or more likely by differences in source regions.

The analyses to this point have been in terms of mean properties, vertically resolved, but these mean properties tell only part of the story. Dust and other aerosol species during ACE-Asia were often found in distinct layers (Kline et al., 2004; Lee et al., 2003) and in different states of mixture. A dramatic example of this is shown by Kline et al. (2004, see Fig. 13 from that paper). In a profile taken over the Yellow Sea, 13 separate layers can be identified over a vertical distance of 5.5 km, based on measured SO_2 and sub- and super-μm light scattering. In the lower layers, sub-μm scattering by pollution is more prevalent, but dust also makes a significant contribution. In the upper layers, dust is dominant, but the layers all have different amounts of SO_2 and sub-μm scattering. The implication is that each layer has a distinct history and composition.

4.5.3. State of mixture and component interactions

The complexity discussed above regarding the vertical distributions of aerosol components makes it difficult to generalize about their interactions. Nevertheless, various types of interactions were observed and these followed certain regular patterns. Below 2 km it was common to encounter dust that had been recently mixed with pollution emitted from eastern Asia. At higher altitudes, dust was less impacted by pollution — for example, the amount of BC in super-μm sizes was less than in the BL.

When dust passes through a region of pollutant emissions, we expect dust surface area to compete with the evolving pollution accumulation mode through coagulation with primary (e.g. BC) and/or uptake of secondary (e.g. sulfur) pollutant species (Tang et al., 2004a,b). During a large dust outbreak, measurements over the Yellow Sea showed that the characteristic time for vapor transfer to the aerosol is very short — about 2 min for the fine mode and 4 min for the coarse mode (Maxwell-Meier et al., 2004). These processes will not only modify dust properties (making the particles both more absorbing and more hygroscopic) but also the properties of the accumulation-mode pollution aerosol. The latter effect is difficult to predict. What was observed in ACE-Asia was that the presence of dust was associated with a reduction in the relative fraction of volatile condensates on the sub-μm soot (BC) and a concurrent lowering of sub-μm ω. Thus, it appears that the loss of scattering material to the super-μm dust was more important than the loss of BC (Clarke et al., 2004). A remaining question is whether the BC that is found at super-μm sizes results primarily from emissions in those size ranges (Shi et al., 2003) or becomes attached to the dust by coagulation, as is evident on some electron microscope images (Clarke et al., 2004; Quinn et al., 2004, see also Section 4.6 below).

The mixing of dust and pollution also affects f_{RH}. Under conditions where dust was dominant, the near surface f_{RH} was reduced in both coarse and fine size ranges (Carrico et al., 2003). The redistribution of soluble species away from accumulation mode pollution particles and onto dust particles was found to cause only a minor increase in dust hygroscopicity but to reduce f_{RH} for the accumulation mode aerosol by up to 40% (Howell et al., 2006). (Note, however, that because the total scattering is dominated by dust under such conditions, the net f_{RH} is reduced only by 10% compared to assumptions of no uptake onto dust.) The small increase in f_{RH} evident under high dust conditions (Carrico et al., 2003) can be explained by the growth of the sub-μm dust particles alone (Howell et al., 2006).

Two general results emerge from this analysis. First, changes in optical properties (ω and f_{RH}) arising from the mixing of pollution and dust are dominated by changes to sub-μm (or accumulation-mode) particles. Second, the assumption of an internal mixture at all sizes appears to cause less than a 10% change in the optical properties of the total aerosol compared to the assumption of externally mixed components under high-dust conditions. This latter result is simply due to

the dominance of the mineral particles on the aerosol optical properties under high dust loads.

4.5.4. Discussion and summary of C-130 results

It is important to note that sampling by the C-130 during ACE-Asia should not be taken as representative of the entire Asian outflow region. First, the sampling was not random, but rather the missions generally involved targeted flights, often with dust encounters as the objective. In addition, the study domain was restricted to northern China such that air masses from southeastern Asian that have strong biomass-burning signals were not sampled.

Despite these limitations, the data succeed in revealing many of the complex features of both aerosol vertical structure and component interactions in this region. They make clear that surface-based in situ measurements often will not provide a reliable indication of column properties. They provide general guidance on how optical properties are modified by component interactions. Finally, the observations of vertical layering and a variety of mixing states imply that when Asian dust and pollution aerosols are transported across the Pacific (e.g., Clarke et al., 2001; Jaffe et al., 2003), they may or may not manifest the effects of component interactions.

4.6. Black carbon and the aggregation of black carbon and dust — results from scanning electron microscope (SEM) analysis

Carbonaceous aerosols are receiving increasing attention owing to their strong radiative forcing effects, but these particles are extremely diverse in physical and chemical characteristics. The most abundant carbonaceous aerosol materials are black carbon (BC) and organic species, but the line between these types is not always sharp (for instance in marine boundary layer samples collected on the NCAR C-130 during ACE-Asia, abundant aggregates of BC, organic carbon, and sulfate were observed by transmission electron microscopy, TEM). Much of the uncertainty about forcing by BC exists with regard to mixing state and internal structure (Chung and Seinfeld, 2002), and these are not well characterized at present for East Asia or in any other important anthropogenic source region.

There is great diversity in BC forms that occur in ACE-Asia aerosols. By far, the most abundant form of BC is the soot produced from combustion, especially the combustion of various grades of coal, which may be affected by different types of control technologies (and open coal burning for household use, common in some parts of China). The soot emitted from the combustion sources is not all well characterized, but a range of spherule sizes and structural arrangements of spherules is to be expected. The size of soot sampled from the NCAR C-130 as determined by high resolution scanning electron microscopy (SEM) and TEM varied from ~10 nm to several hundred nm. The density and structure of aggregation of the spherules was also seen to be highly variable. SEM micrographs of two examples are shown in Fig. 8.

A striking feature of the East Asia outflow evident from studies onboard the NCAR C-130 and at the ground sites on Jeju Island was the extensive aggregation of BC and dust apparent in SEM images. An example of a BC/dust aggregate is shown in Fig. 9. Image analysis of the dust and BC populations and their aggregation and overlap showed that typically 15% to 30% of a dust particle's surface was covered by BC. For

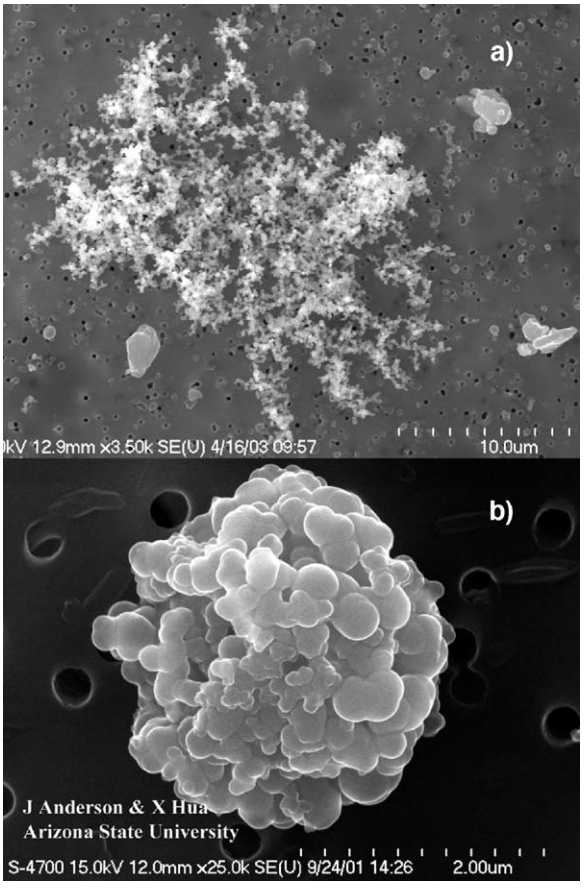

Fig. 8. Field emission SEM images of: (a) closely packed soot with large spherules, East Asia outflow collected from R/V Ronald Brown on March, 25, 2001 from over the Pacific Ocean east of Japan; and (b) large open soot particle collected from NCAR-C-130 on April 27, 2001 above Sea of Japan. Holes are 0.4 μm pores in membrane filters.

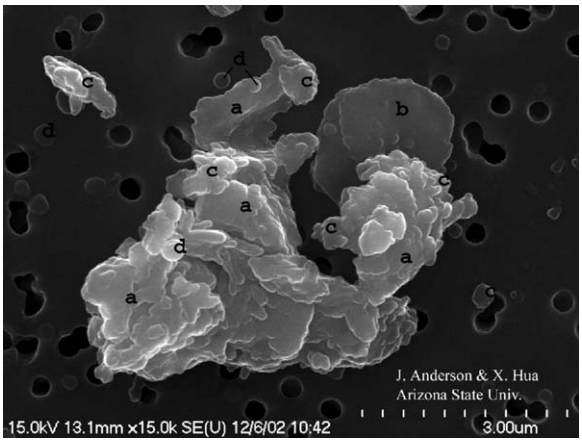

Fig. 9. Field emission SEM image of RF13 sample from 600 m leg over Yellow Sea. Large central particle is a silicate dust/black carbon aggregate consisting of: (a) Ca aluminosilicate, (b) Mg aluminosilicate, (c) black carbon spherule aggregates (soot), (d) separate carbon spheres.

instance, for C-130 Flight RF13 on April 23, 2001 individual particle samples were analyzed from three level-legs over the Yellow Sea. The percentages of dust particle surfaces covered by BC in these samples were 19.5%, 27.4%, and 21.7% for the 250, 600, and 5500 m legs, respectively. The arithmetic means of the average diameters for each particle (that is, the minimum plus maximum diameters divided by two) of dust, total BC, and BC particles aggregated with dust were as follows: (at 250 m altitude) 2.39 μm, 0.38 μm, 0.46 μm; (600 m) 2.56 μm, 0.41 μm, 0.51 μm; (5500 m) 1.99 μm, 0.40 μm, 0.52 μm. From size and shape data, the aggregated BC particles appear to be a subset of the total BC population; that is, other types of BC were aggregated with dust and certain types were not.

There is much to be learned about how the dust/BC aggregation occurs, but regardless of the underlying mechanisms, there are potentially important implications for radiative forcing. Clearly the partial coverage of dust particles by BC makes the internal mixtures more absorbing of visible and infrared radiation; and this should be reflected in a decrease in ω. Thus, the net negative forcing characteristic of unadulterated dust particles will be diminished by mixing with BC. The samples from C-130 RF13 are typical, not isolated examples, and as noted above (Section 4.3), the net forcing by Asian dust can be more accurately quantified if the extent of dust/BC aggregation and the effects of mixing on ω can be better constrained. Of course, aggregation with other aerosol components such as ammonium sulfate also will affect the radiative properties of the dust and pollution aerosol as well as the lifetimes of the various chemical components in the mixtures.

4.7. Modeling the radiative properties of Asian dust

The results from ACE-Asia along with other recent dust-related field experiments (e.g., the Puerto Rican Dust Experiment, PRIDE, the Saharan Dust Experiment, SHADE, and the Asian Dust ADEC) all indicate that dust particles have complex shapes and composition that vary with particle size. This complexity renders the prediction of dust radiative properties difficult.

Kalashnikova and Sokolik (2004) proposed a new approach to model the optical properties of particles of complex shape and composition such as mineral dust. In contrast to previous studies that assume a model shape (spheroid or sphere), this approach considers mineral dust as a mixture of particles characterized by the representative composition-shape-size distributions (CSS) that are reconstructed from TEM/SEM microscopy, mass spectroscopy or other measurements that provide information on individual particles. Then the optical characteristics of CSS are computed using the Discrete Dipole Approximation (DDA) technique. This approach was applied to the data collected during the ACE-Asia experiment (Sokolik et al., 2003) as well as to a unique data set of physicochemical properties of Asian dust measured in a wind-tunnel experiment (Lafon et al., 2004).

The modeling results revealed that nonspherical dust particles tend to have a higher single scattering albedo relative to volume-equivalent spherical particles. Furthermore, nonspherical particles result in very different scattering phase functions. The latter is especially important in remote sensing (Kalashnikova et al., 2005) as well as for the interpretation of in situ optical measurements based on the principle of light scattering such as optical particle counters and nephelometers (Reid et al., 2003). The significant impact of dust nonsphericity on the angular distribution of scattered intensity has also been confirmed by measurements made as part of the Aerosol Robotic Network, AERONET (Dubovik et al., 2000).

The studies of Lafon et al. (2004, in press) used new data on the amount of iron oxides in Asian dust to provide an additional constraint to its ability to absorb light in the visible region. These authors show that the aggregates of iron oxides and clays, which are a key light absorbing species of mineral dust, can have effective refractive indices ranging from about 3.8×10^{-5} (for "pure" kaolinite) to about 4.6×10^{-3} (for aggregates with 2% hematite) at 550 nm. This variability is mainly due to differences in source-

dependent "free" iron content and the speciation of iron oxides and clay minerals (Lafon et al., in press). Given that Asian dust mixtures consist of iron oxide/clay aggregates as well as several other minerals (e.g., quartz, calcite), which do not or weakly absorb light in the visible, the effective absorption of the Asian dust is expected to be lower on a per unit mass basis than that of iron oxides/clay aggregates.

Fig. 10 shows an example of the spectral dependence of ω calculated with the new data on mineralogical composition of Asian dust (Lafon et al., in press). Here ω calculations are done for spherical particles having a representative two-size mode lognormal distribution. Also shown is the ω calculated using the refractive indices of Patterson et al. (1977) and the OPAC dust-like model (Hess et al., 1998) for the same size distribution; these sets of refractive indices are commonly used in to model dust radiative forcing. The various differences in ω are apparent in Fig. 10, especially in the spectral behavior. Unfortunately, the latter cannot be directly compared against in situ optics measurements due to a lack of multi-wavelength absorption observations. Indeed, constraining the spectral dependence of ω will be critical to both radiative energy balance calculations as well as atmospheric photochemistry modeling, such as calculations of photolysis rates (Sokolik et al., 2001).

Lower light absorption of Asian dust, compared to that predicted from Patterson's refractive index, is likely to cause more negative, solar, direct, top of the atmosphere (TOA) radiative forcing. However, over the bright surfaces such as snow or clouds, even weakly-absorbing aerosols can result in a positive radiative forcing. Given the persistent cloud cover over East Asia and the North Pacific, constraining the vertical distribution of dust and clouds becomes an important issue. To some extent this might explain the contradictory results reported by recent assessments of the TOA radiative forcing during the ACE-Asia time period. For instance, Conant et al. (2003) predicted negative TOA radiative forcing in the presence of dust outbreaks, whereas a study by Takemura et al. (2003) reported positive radiative forcing over some regions. Furthermore, there are significant differences in the spatial pattern of TOA radiative forcing predicted by these studies that are likely due to different chemical transport models used. It becomes clear that improved quantification of dust radiative impacts would require both a more realistic treatment of dust optics as well as better prediction of a spatio-temporal distribution of atmospheric dust and clouds.

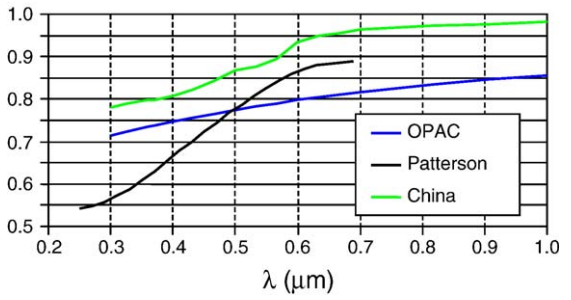

Fig. 10. Spectral dependence of the single scattering albedo for a mixture of light absorbing and non-absorbing minerals representative of Asian dust (green curve). The black and blue curves show the single scattering albedo calculated with Patterson's and OPAC refractive indices, respectively, for the same size distribution (see further details in Lafon et al., in press).

4.8. Chemical transport models

4.8.1. Asian dust emissions and transport

Three models provided forecast information to support the ACE-Asia experiment from March 30 to May 4, 2001: the Goddard Chemistry Aerosol Radiation and Transport (GOCART) model (Chin et al., 2002, 2003), the Model of Atmospheric Transport and Chemistry (MATCH), and the Chemical Forecast (CFORS) model (see Huebert et al., 2003 for an overview). During ACE-Asia, several dust outbreaks occurred, and some of the dust plumes traversed the North Pacific, eventually reaching North America. Fig. 11 shows such a trans-Pacific dust transport episode predicted with the GOCART model (left panel) and detected by the satellite-borne Total Ozone Mapping Spectrometer, TOMS (right panel).

On April 8, a major dust outbreak originating mainly from the Gobi and the Mongolian plateau was transported downwind to the Pacific. At the same time, there was a second branch of dust wrapping around a low-pressure system at 50°N, 125°E (top panel, left column in Fig. 11). The prevailing northwesterly winds over central China and southwesterly winds near the east coast turned the dust plume from a west–east direction on April 8 to a southwest–northeast direction on April 11, with dust plume penetrating as far south as 20°N over eastern China (middle panel). The dust plume meandered across the Pacific Ocean, and on April 14, the entire west coast of North America from 30°N to 60°N was heavily influenced by the dust from Asia (bottom panel); it then moved further inland. As shown in Fig. 11, the model and the TOMS aerosol index (TOMS-AI) have similar patterns of dust plume evolution and long-range transport.

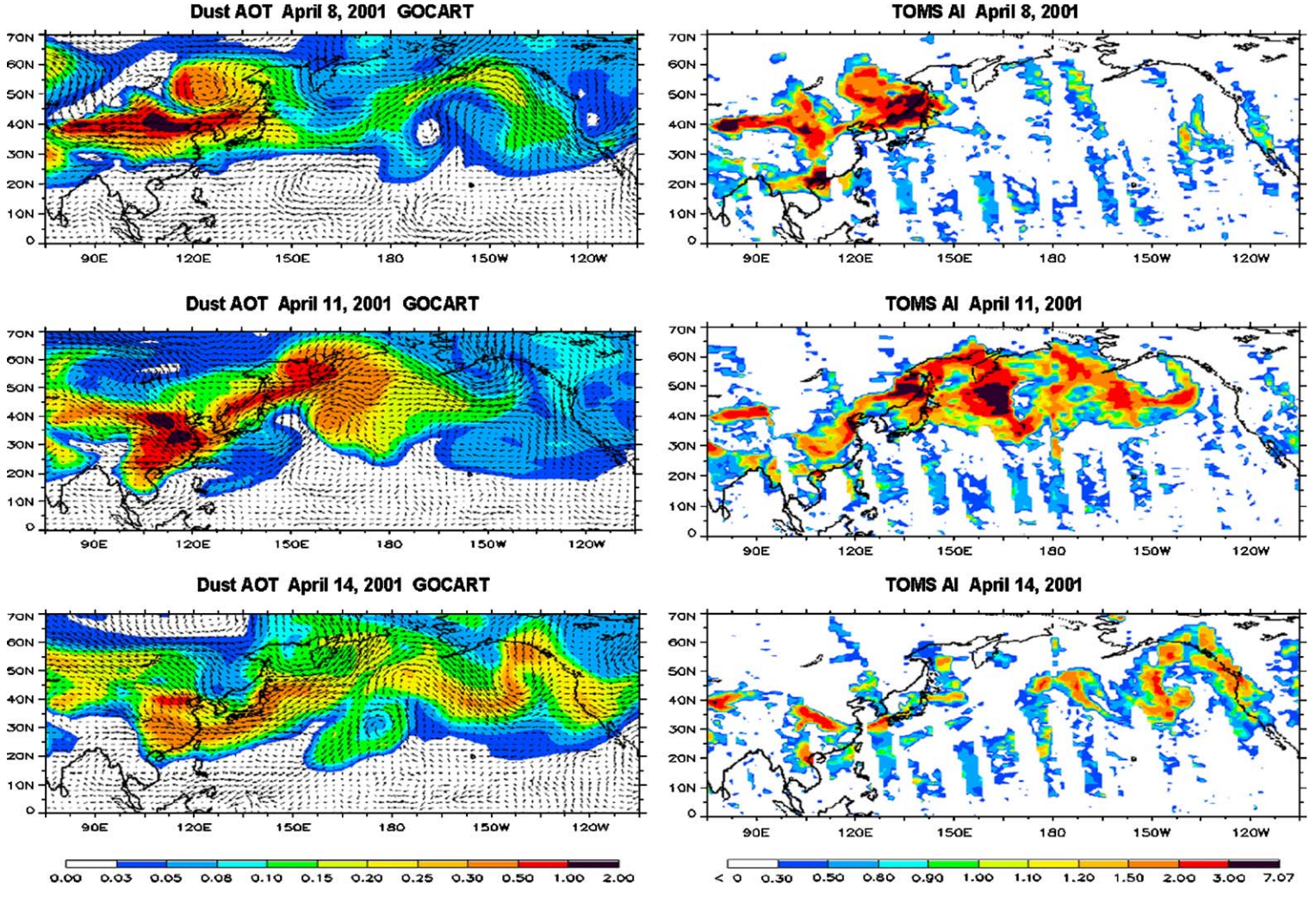

Fig. 11. Dust evolution and trans-Pacific transport (shown as aerosol optical thickness or AOT at 550 nm) and the TOMS aerosol index (AI) on April 8, 11, and 14 in 2001.

Dust plumes originating from Taklimakan and Gobi deserts usually travel above the boundary layer because of the high elevation of these deserts (>2 km above sea level). If captured by a strong easterly jet, these plumes can travel long distances as illustrated above. On the other hand, large concentrations of dust in the boundary layer were often observed during ACE-Asia over the Yellow Sea, with concentrations sometimes exceeding 200 μg m^{-3}. All three models that supported ACE-Asia field operations had predicted the high-altitude dust plumes, but none had forecasted the high dust concentrations observed in the boundary layer over the Yellow Sea shown in Fig. 12. Fig. 12a is the dust emission for April 2001 predicted by the GOCART model during the forecast period; it was calculated based on the surface winds, wetness, and the probability of dust uplifting, which was defined by the degree of surface depression with bare vegetation coverage (Ginoux et al., 2001). Using the sources shown in Fig. 12a, the model predicted the dust concentrations below 2 km would be 10 to 20 μg m^{-3} while the Total Aerosol Sampler (TAS) on the C-130 aircraft detected much higher concentrations, 40 to 200 μg m^{-3}.

The model underprediction of boundary layer dust over the Yellow Sea led to an investigation of possible "missing sources" for dust over Asia. As a first step, we used the vegetation coverage from the 1987 AVHRR land cover data (DeFries and Townshend, 1994) to ascertain if the surface is "bare" or covered by vegetation in the model. However, it has been recognized in recent years that China has experienced desertification (e.g. United Nations Convention to Combat Desertification or UNCCD, http://www.unccd.de), especially in Inner Mongolia. To test the possible impact of dust emissions from the desertified regions, we consulted maps on desertification in China (CCICCD, 1997), and evaluated the dust sources in Inner Mongolia, east of 110°E. These areas have been suffering from overgrazing and drought in recent years. As a consequence, they have become "bare soil" instead of "grassland" as classified in the 1987 AVHRR land cover map.

The modified dust emission in April 2001 is shown in Fig. 13a, and the model calculated dust concentration over the Yellow Sea with this modified dust source in Fig. 13b. The addition of the Inner Mongolia desertification sources made a significant difference in model-calculated dust vertical distributions over the Yellow Sea. This is because dust emitted from this region is readily advected to the Yellow Sea, contributing mostly to the low-altitude dust loads. Compared with the model forecast product shown in Fig. 12b, it is apparent that this refinement of the model led to a much better agreement with the observations.

4.8.2. Regional dust budget studies during using the CFORS model

A regional-scale aerosol transport model, the Chemical weather FORecasting System (CFORS), was used for the analysis of large-scale dust phenomena during the ACE-Asia IOP. Dust modeling results were examined and compared with surface weather reports, the TOMS-AI, Mie scattering Lidar observations, and surface aerosol observations (Uno et al., 2004). The CFORS results accurately reproduced many of the

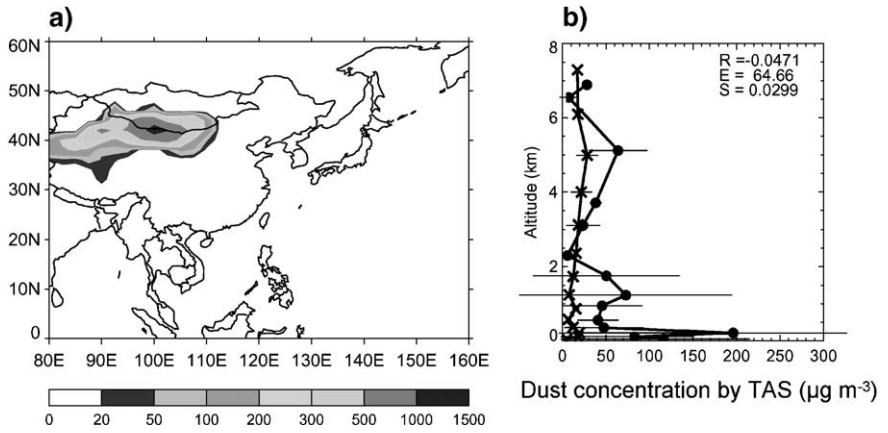

Fig. 12. (a) Dust emissions (mg m^{-2} day^{-1}) in April 2001 from the GOCART model during ACE-Asia forecast. (b) Dust vertical profiles over the Yellow Sea predicted by the GOCART model (X's) using the source in (a) and measured by the Total Aerosol Sampler (TAS) on the C-130 aircraft (filled circles) during ACE-Asia. *R* stands for correlation coefficient for observed versus predicted, *E* for root mean error and *S* for model forecast skill score. The TAS data are from B. Huebert, U. Hawaii.

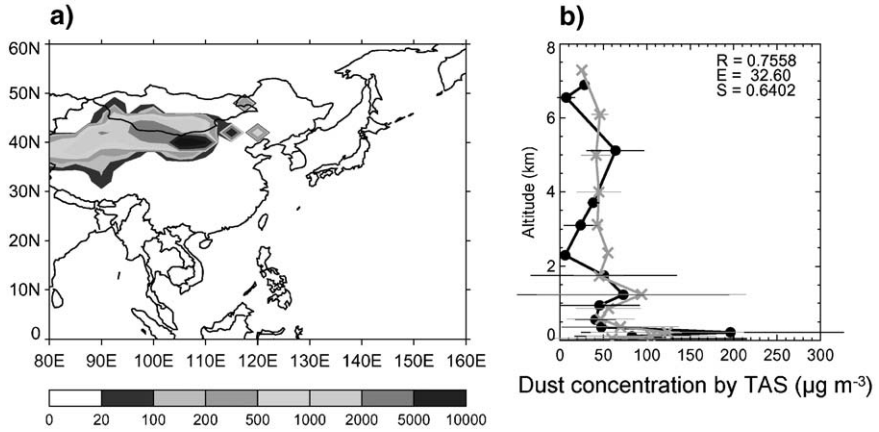

Fig. 13. (a) Dust emissions (mg m^{-2} day^{-1}) in April 2001 with modified source from the GOCART model. (b) Dust vertical profiles over the Yellow Sea calculated with the GOCART model (gray, X's) using the source in (a) and measured by the Total Aerosol Sampler (TAS) on the C-130 aircraft (black, filled circles) during ACE-Asia. *R*, *E* and *S* as in Fig. 12. The TAS data are from B. Huebert, U. Hawaii.

important observed features of the dust events. For example, a quantitative examination of aerosol optical depths showed that model predictions were within ~20% of the Lidar observations for the major episodes. Time variations of the CFORS dust fields showed the correct onset timing of the elevated dust concentrations for a group of surface observation sites. Here we summarize the regional dust budget based on the CFORS model.

The major dust outbreaks during the spring of 2001 can be classified as follows: DS1 (March 2 to 7), DS2 (March 18 to 25), and DS3 (April 4 to 14). These major dust episodes are similar to those reported by Gong et al. (2003), but those authors also considered a fourth event which occurred from late April to early May (see below). Similarly, Liu et al. (2003a,b) targeted the large-scale dust episode covering the DS3 period with a very high-resolution dust transport model.

The structure of the PDS was investigated using the CFORS model, and we found it instructive to divide DS3, into two parts: DS3-1 and DS3-2. The model showed two layers of dust in the BL and one aloft. The higher-altitude dust layer was linked to the movements of two large low-pressure systems: that dust layer originated over the Taklimakan desert area on April 7 to 8, and it was transported to the Sea of Japan on April 9 to 10 (Uno et al., 2004). During DS3-1, the major dust transport pathway was located around 40°N to 45°N, and the dust transported at 6 km was an important feature of this event.

The structure of DS3-2 was quite different than DS3-1. During DS3-2, a southern branch of PDS was located at 30°N and 36°N while second transport pathway was located farther north between 46°N and 50°N at an altitude of 1 to 4 km. Understanding such a complicated structure of the dust plumes is very important for identifying dust sources and for evaluating the variations in dust concentrations observed on the various ACE-Asia sampling platforms, especially the mobile NCAR C-130 and the RHB platforms.

Total emissions during the simulation period calculated from the CFORS model between March and April, 2001 were estimated to be 105 Tg for mineral dust particles with diameters, $d<40$ μm. Dry deposition, gravitational settling, and northward outflow of mineral dust account for 33%, 27%, and 13% of the total emission, respectively. Dust total deposition processes play a major role in the overall budget relative to the dust subject to long-range transport.

The dust flux at 130°E longitude is important for evaluating the importance of the dust flux from China to Korea, Japan, and the Pacific Ocean (covering the ACE-Asia observational domain). The mean cross sections of the longitudinal dust transport fluxes from the west to east across longitude 130°E for each dust episode of DS3 are shown in Fig. 14. That figure also includes the average dust concentrations, which are shown as contour lines.

The calculated amounts of dust transported across 130°E (with the fraction of the total flux in parentheses) for DS1, DS2, DS3-1, and DS3-2 were 7.9 Tg (14.3%), 10.9 Tg (19.7%), 6.1 Tg (11.1%), and 12.5 Tg (22.7%), respectively. The dust transport had a strongly intermittent quality because of the cold front activities. It is notable that 68% of the dust flux during March and April 2001 occurred during the three major dust episodes, and approximately 34% of total dust transport occurred during DS3. Overall, the total amount of dust

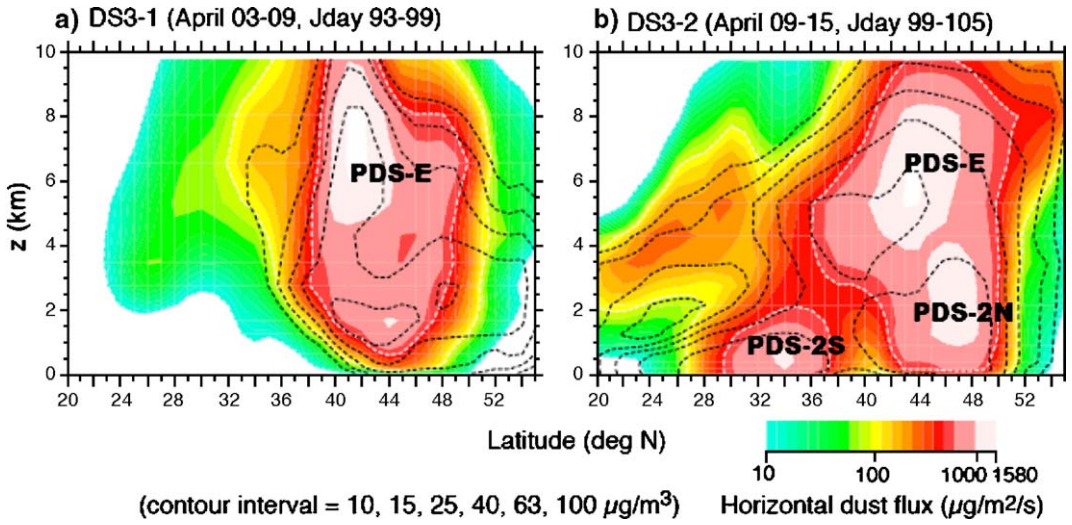

Fig. 14. Average dust concentration (lines) and horizontal dust transport flux (contours) averaged over the dust episodes along 130°E longitude. PDS stands for Perfect Dust Storm.

transported across 130°E during March and April was estimated to be 55.2 Tg.

The major conclusions from this study agree qualitatively with the work of Liu et al. (2003a,b) and Gong et al. (2003 and below). However, the estimated dust fluxes and concentration levels do differ among models, and this fact emphasizes the necessity of further studies to clarify models' sensitivity to the dust emission scheme, the horizontal/vertical resolution, uncertainties in surface land use/soil texture information for the specification of dust emission area, and dust removal mechanisms.

4.8.3. Trans-Pacific transport of Asian dust aerosol

A size segregated soil dust emission and transport model (the Northern Aerosol Regional climate Model, NARCM) (Gong et al., 2003) was used to simulate the trans-Pacific transport of Asian dust during the ACE-Asia spring 2001 period. The model is driven by the NCEP re-analyzed meteorology and includes the following atmospheric aerosol physical processes of soil dust: production, transport, growth, coagulation, and dry and wet deposition. A Chinese soil texture map that infers the soil grain-size distribution with 12 categories was generated to drive the modified size distributed soil dust emission scheme (Alfaro et al., 1998; Marticorena and Bergametti, 1995).

The ACE-Asia experiment provided a large number of observations for model evaluation, and the NARCM-simulations were compared with ground-base measurements in East Asia and North America and with satellite measurements. The modeling results captured most of the dust mobilization episodes during this period in China, and the model reasonably simulated the concentrations in source regions and downwind areas from east China to western North America (Figs. 15 and 16). About 252.8 Tg of soil dust for particles with diameters, $d<41$ μm was estimated to be emitted in the East Asian deserts in spring (March to May) 2001. This is roughly 2.5 times that predicted by CFORS for March and April as presented above. Approximately 60% of the dust flux was attributed to four major dust storms (1) March 2 to 6, (2) March 20 to 25, (3) April 6 to 14, and (4) April 29 to May 5, 2001. The vertical dust loadings above 700 hPa correlate reasonably well with TOMS-AI observations spatially and temporally, and the trans-Pacific transport of Asian dust was clearly identified (Fig. 16). These analyses showed that the trans-Pacific transport of Asian dust is largely controlled by the strength and orientation of the major East Asian trough system. The modeled trans-Pacific transport of Asian dust and its intrusion into North America in April 2001 show good agreement with ground and aircraft observations made in the vicinity of the Olympic Peninsula and Saturna Island, Canada (Fig. 17, see also Gong et al., 2003).

Implications for trans-Pacific transport with modeled size-segregated Asian dust emission, deposition and budgets during ACE-Asia 2001 were also investigated from the NARCM-modeling (Zhao et al., 2003). Simulated mass size distributions of deposition in the source region were similar to those of the dust emissions, both showing a diameter peak around 4 to 5 μm. Over the dust transport pathway, far from the

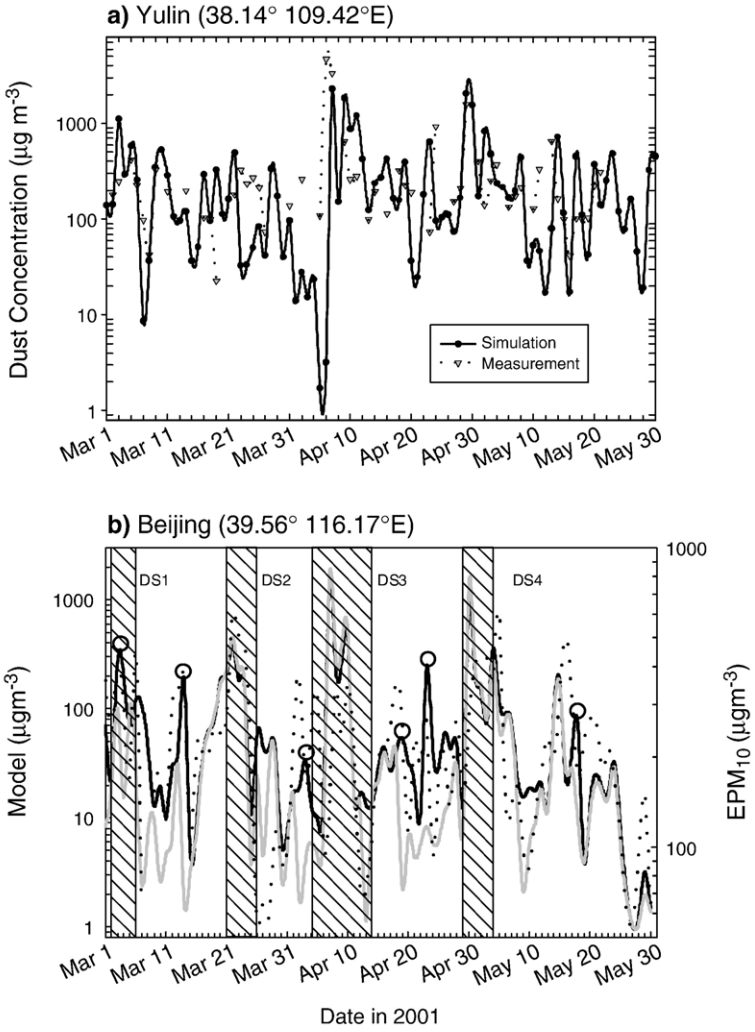

Fig. 15. Comparisons of modeled surface dust concentrations in China with (a) the surface measured dust concentrations at Yulin and (b) air quality index derived PM_{10} (EPM_{10}) concentrations at Beijing. The two curves in (b) represent simulations using input from the EROS satellite data (gray line) and CDM (China Desertification Map)+EROS data (black line), respectively. The open circles on the plot identify the improvements of the CDM+EROS data set to correctly predict the dust peaks. Local time is used for the plots. The four major dust storms in spring are shown as DS1, DS2, DS3 and DS4.

source region, the size distributions of dust deposition showed substantial decreases: there the peak diameters were 1 to 3 μm. It is noteworthy that these peak diameters are towards the smaller range of values (mean value of 4.5±1.3 μm) for aerodynamic mass-median diameters for various regions compiled by Reid et al. (2003).

Dry deposition is the dominant removal process over the source regions and nearby areas. In contrast, along the pathway of the trans-Pacific transport far from the source regions, for example over the North Pacific, wet deposition exceeds dry deposition by up to a factor of 10 (Fig. 18). Indeed, the model indicates that wet deposition is the major process for dust removal from the atmosphere over the North Pacific, and this supports results obtained during an early study of air/sea dust exchange in that region (Uematsu et al., 1985).

The monthly averaged Asian dust outflow from the East Asian subcontinent showed peak transport at 38°N in March; 42°N in April, and 47°N in May. Furthermore, dust was lifted from < 3 km in the lower troposphere in East Asia to ~6 km in the middle troposphere over the North Pacific and western North America. In March the transport-axis extended around 30°N and 40°N from East Asia to the North Pacific while

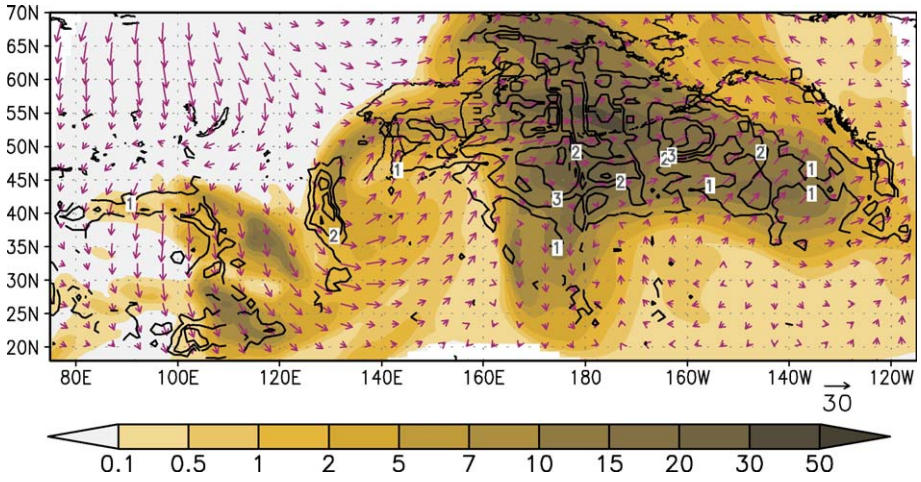

Fig. 16. Daily dust loading (ton km^{-2}) above 700 hPa (filled contours) from the NARCM and the TOMS-AI-measurements (black lines) on April 12, 2001. Wind vectors (m s^{-1}) are at 500 hPa.

in April a zonal transport pathway around 40°N was well developed over the North Pacific and reached North America. In May, the transport separated into an eastward zonal path over North Pacific and a meridional path from the source regions to the northeastern part of the continent. Desert areas in western and northern China and Mongolia were found to be the largest contributors to the dust transport: the regionally averaged dust emission was estimated to be 21.5 t km^{-2} with a net export of 8.42 t km^{-2} for March to May. The regions from the Loess Plateau to the North Pacific are shown to be dust sinks, with the Loess Plateau a major sink, receiving 5.84 t km^{-2} in the spring.

4.9. Asian dust storms: health effects in Seoul, Korea

Although dust storms have been studied for many years, they have historically been considered natural phenomena, and their impacts on human activities have generally been considered mainly a nuisance. More recently, the potential effects of dust storms on human health and air quality have been recognized, and public concerns over the health effects of dust storms have been increased dramatically in the past 5–10 years.

Kwon et al. (2002) evaluated the relationship between the records of daily mortality and dust storm events in Seoul, Korea. These authors collected the daily mortality data, excluding accidental deaths, and then evaluated this information with reference to records of dust storms and other meteorological conditions between 1995 and 1998. Also included in their evaluation were concentration data for various atmospheric trace species. These studies showed that the PM_{10} mass concentration was the only variable that exhibited different values, with statistical significance ($p<0.01$ based on a *t*-test), between the non-dust storm (73.3 μg m^{-3}) and the dust storm periods (101.1 μg m^{-3}). Their results provide weak, but intriguing evidence that the dust storms are associated with increased risk of death from all causes (1.7% increase in the rate of deaths from 3-day moving average of exposure with a 95% confidence interval of −1.6 to 5.3). Moreover, the association was stronger for the deaths due to cardiovascular and respiratory causes (4.1% increase with a 95% confidence interval of −3.8 to 12.6). Thus, in this pioneering study of possible health affects associated with Asian dust, the authors concluded that the persons with advanced cardiovascular and respiratory disease may be particularly susceptible to the effects of dust storms.

5. Concluding remarks

More than sixty papers resulting from studies conducted as part of ACE-Asia have been published in the *Journal of Geophysical* research alone, and clearly the summaries of results presented here could not begin to cover all of the mineral dust research done for the program. Despite these limitations, the results presented above show how the aerosol concentrations change over time and how they vary in 3-dimensions. The summaries provide information on dust budgets and fluxes and also highlight some of the principal interactions involving various atmospheric constituents. The ground-based results and especially the aircraft

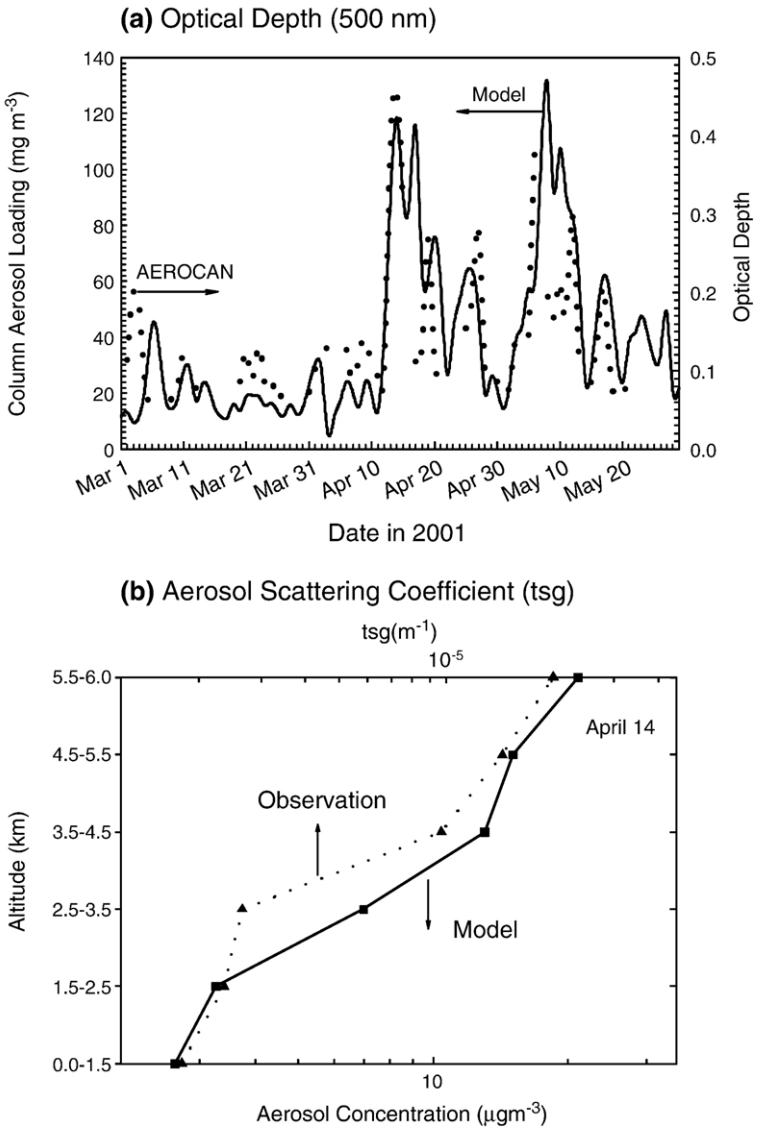

Fig. 17. Comparisons of NARCM-simulations with North American measurements of (a) optical depth at Saturna Island, Canada by AEROCAN (the Canadian sunphotometry network) and (b) submicron aerosol scattering coefficient (tsg) at Cheeka Peak, USA on April 14, 2001. The arrows in both figures point to the '*Y*' or '*X*' axis appropriate for each curve.

studies make it clear that surface-based measurements of aerosol properties often are decoupled from those above the boundary layer.

Sokolik et al. (2001) noted that uncertainties in the radiative effects of dust will be reduced as the models' dust emission schemes improve, the distributions and transport of dust in the models become more realistic, and the dust removal mechanisms are better handled. A recent intercomparison of dust models shows that there still remain substantial differences in current models with respect to dust emissions (Zender et al., 2004), and as noted above, there are substantial uncertainties in the mass budgets for Asian dust. As illustrated by the GOCART model results presented here, the accuracy of the dust models will likely co-evolve with the sophistication of the measurements and as various databases develop. In the case of the GOCART model, the recognition of new dust sources was driven by the unexpectedly high dust concentrations seen aboard the C-130 aircraft.

Impressive amounts of field data on the physical, chemical and optical properties of aerosols from Asia have been collected for ACE-Asia and related programs, and both laboratory and radiative modeling studies have

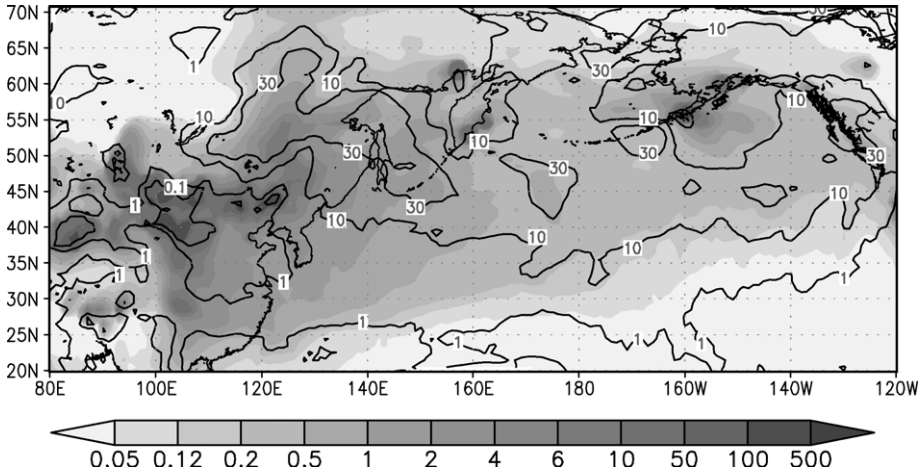

Fig. 18. Total deposition (filled contours, ton km^{-2}) and ratio of wet to dry deposition (contour lines) for spring 2001.

begun evaluating the properties of the dust that lead to uncertainties in climate assessments. As noted here, two characteristics of the dust are particularly important in this regard: the presence of naturally occurring light-absorbing substances, such as iron-oxides, and the nonsphericity of the particles. Although some progress made in addressing these issues (e.g., Arimoto et al., 2002; Dubovik et al., 2002; Mishchenko and Travis, 2003; Lafon et al., 2004, respectively), a better understanding of dusts' optical properties remains one of the keys to reducing the uncertainties in the radiative impacts of dust both for present-day climate and for future scenarios. These uncertainties also will be reduced as progress is made in our ability to model the interactions of dust and with clouds and with other types of aerosol plumes.

Yet another critical uncertainty concerns the interactions of dust with pollutants and the effects of mixing state on the dust aerosol. Studies at Gosan and Zhenbeitai conducted for ACE-Asia showed that aerosol concentrations and properties are strongly affected by the occurrence of Asian dust storms and that the dust is commonly mixed with biomass burning and coal combustion products. Studies at surface sites have also provided some insights into the integrated effects of mixing on aerosol properties and composition, showing for example that light-absorbing pollutants typically are added to dust plumes during transport, and that the concentrations of some anthropogenic substances, specifically Pb, NO_3^- and SO_4^{2-} can be higher during dusty periods than under non-dusty conditions. Ground station data also show that various water-soluble cations (Na^+, K^+, Ca^{2+}, Mg^{2+}) are well correlated with elemental indicators of dust and that distinct differences exist between the Ca/Al, Si/Ca, and Fe/Ca ratios in Asian dust versus African dust.

The summaries of the ATOFMS data collected on the RHB showed that in post-frontal air, most of the supermicrometer nitrate and sulfate was associated with mineral particles. More detailed analyses of the ATOFMS data provide some original and unexpected insights into how these associations arise. Most revealing were analyses showing that single dust particles typically do not contain large amounts of both sulfate and nitrate (or both sulfate and chloride), but rather one species to the exclusion of the other (Sullivan et al., in press). Therefore, the processes responsible for the mixing or production of these substances appear to be competitive in nature. Such selective reactivity has not been previously reported for ambient dust aerosols.

The summaries of results obtained with the C-130 aircraft vividly illustrate how the optical properties of the aerosol can be modified when pollutants interact with dust. This is important because the mixing of dust with fine pollution particles and the chemical reactions of dust with gas-phase species ultimately become manifest as influences on radiative forcing. In addition to the optical effects, the atmospheric lifetimes of all substances involved in the reactions and mixing will be altered in complex and as yet largely undetermined ways, and these effects clearly deserve more detailed study. Nevertheless, the ACE-Asia C-130 data, even though restricted in scope, indicate that the effects of mixing on aerosol optical properties are likely more important for the fine pollution mode particles (and the fine particles that would otherwise form if the gas–dust particle reactions had not occurred) than for the coarse dust particles.

In addition the transfer of fine particles and volatiles to the coarse dust, there is overwhelming evidence that dust and BC form aggregates, and there are potentially important implications of such internal mixing for radiative forcing. Aggregation with BC will make the dust particles more absorbing of visible and infrared radiation, thus lowering the single scattering albedo. Interestingly, as noted in Section 4.6, SEM analyses demonstrate that the aggregation of BC particles with dust appears to involve a selective process, but a more central issue is whether the presence of soot significantly affects the optical properties of the dust. The aerosol optical studies conducted aboard the C-130 and summarized here indicate that coarse dust is the major light absorber and that the optical effects of the soot mixing with dust are a second-order concern. On the other hand, analyses of SEM images suggest that the consequences of mixing may be more important.

While it was impossible in this summary paper to critically review and inter-compare all of the relevant optical and SEM data on BC/dust aggregates and the associated effects on light extinction, it is obviously desirable to better constrain the extent to which BC/dust aggregates affect light scattering and absorption. As a first step, comparative studies of data obtained by different methods are needed, but such studies would be challenging because the samples would have be precisely matched to cover same range of particle sizes, and they would have to be matched to cover the same sampling interval. Alternatively, it is possible that some appropriately designed studies, perhaps involving overdetermined data sets, could be developed to evaluate the importance of BC/dust aggregates with respect to the fluxes of radiant energy.

It has been suggested that the last few years of the 20th and early part of the 21st century may someday be regarded as the "golden age" of dust research (Y. Shao, City University of Hong Kong, personal communication). ACE-Asia was one of several large international collaborative programs that brought together scientists who shared an interest in investigating how Asian dust particles are generated and transported, how the dust interacts with other atmospheric constituents, and more generally how dust is linked to climate. The summaries presented here cover only a small fraction of the research done for the program. Nonetheless, we hope that the ACE-Asia will be viewed as an important step towards reducing the uncertainties in the effects of dust on the Earth's climate systems, first by expanding our general understanding of atmospheric dust in relation to climate and second by improving our ability to model its formation, chemical reactions, transport, and deposition.

Acknowledgments

The authors are pleased to acknowledge the contributions of the innumerable scientists and support personnel who contributed to the overall success of the ACE-Asia program but who unfortunately cannot be individually recognized here. Financial support for ACE-Asia was provided by at least thirty-five groups from eight different countries, and that generous support is a pleasure to acknowledge as is the collaborative spirit of all ACE-Asia investigators. This paper is a contribution to the International Global Atmospheric Chemistry (IGAC) Core Project of the International Geosphere Biosphere Program (IGBP) and part of the IGAC Aerosol Characterization Experiments (ACE).

References

Alfaro, S.C., Gaudichet, A., Gomes, L., Maille, M., 1998. Mineral aerosol production by wind erosion: aerosol particle sizes and binding energies. Geophys. Res. Lett. 25, 991–994. doi:10.1029/98GL00502.

Alfaro, S.C., Gomes, L., Rajot, J.L., Lafon, S., Gaudichet, A., Chatenet, B., Maille, M., Cautenet, G., Lasserre, F., Cachier, H., Zhang, X.Y., 2003. Chemical and optical characterization of aerosols measured in spring 2002 at the ACE-Asia supersite, Zhenbeitai, China. J. Geophys. Res. 108 (D23), 8641. doi:10.1029/2002JD003214.

An, Z.S., Liu, T.S., Lu, Y.C., Porter, S.C., Kukla, G., Wu, X.H., Hua, Y.M., 1990. The long-term paleomonsoon variation recorded by the loess-paleosol sequence in central China. Quat. Int. 718, 91–95.

Anderson, T.L., Masonis, S.J., Covert, D.S., Ahlquist, N.C., Howell, S.G., Clarke, A.D., McNaughton, C.S., 2003. Variability of aerosol optical properties derived from in situ aircraft measurements during ACE-Asia. J. Geophys. Res. 108 (D23), 8647. doi:10.1029/2002JD003247.

Andreae, M.O., 1983. Soot carbon and excess fine potassium: long-range transport of combustion-derived aerosols. Science 220, 1148–1151.

Angelino, S., Suess, D.T., Prather, K.A., 2001. Formation of aerosol particles from reactions of secondary and tertiary alkylamines: characterization by aerosol time-of-flight mass spectrometry. Environ. Sci. Technol. 35, 3130–3138.

Arimoto, R., Duce, R.A., Ray, B.J., Ellis Jr., W.G., Cullen, J.D., Merrill, J.T., 1995. Trace elements in the atmosphere over the North Atlantic. J. Geophys. Res. 100, 1199–1213.

Arimoto, R., Duce, R.A., Savoie, D.L., Prospero, J.M., Talbot, R., Cullen, J.D., Tomza, U., Lewis, N.F., Ray, B.J., 1996. Relationships among aerosol constituents from Asia and the north Pacific during PEM-West A. J. Geophy. Res. 101, 2011–2023.

Arimoto, R., Balsam, W., Schloesslin, C., 2002. Visible spectroscopy of aerosol particles collected on filters: iron oxide minerals. Atmos. Environ. 36, 89–96.

Arimoto, R., Zhang, X.Y., Huebert, B.J., Kang, C.H., Savoie, D.L., Prospero, J.M., Sage, S.K., Schloesslin, C.A., Khaing, H.M., Oh, S.N., 2004. Chemical composition of atmospheric aerosols from

Zhenbeitai, People's Republic of China, and Gosan, South Korea, during the ACE-Asia. J. Geophy. Res. 109, D19S04. doi:10.1029/2003JD004323.

Bates, T.S., Quinn, P.K., Coffman, D.J., Covert, D.S., Miller, T.L., Johnson, J.E., Carmichael, G.R., Guazzotti, S.A., Sodeman, D.A., Prather, K.A., Rivera, M., Russell, L.M., Merrill, J.T., 2004. Marine boundary layer dust and pollution transport associated with the passage of a frontal system over eastern Asian. J. Geophys. Res. 109 (D19), D19S19. doi:10.1029/2003JD004094.

Cahill, T.A., Goodart, C.J., Nelson, W., Eldred, R.A., Nasstrom, J.S., Feeney, P.J., 1985. Design and evaluation of the DRUM impactor. In: Ariman, T., Veziroglu, T.N. (Eds.), Proceedings of the International Symposium on Particulate and Multiphase Processes. Contamination Analysis and Control, vol. 2. Hemisphere, Washington, D.C., USA, pp. 319–325.

Carpenter, G.A., Grossberg, S., Rosen, D.B., 1991. Art 2-a — an adaptive resonance algorithm for rapid category learning and recognition. Neural Networks 4, 493–504.

Carrico, C., Kus, P., Rood, M., Quinn, P., Bates, T., 2003. Mixtures of pollution, dust, seasalt, and volcanic aerosol during ACE-Asia: Aerosol radiative properties as a function of relative humidity. J. Geophys. Res. 108 (D23), 8650. doi:10.1029/2003JD003405.

Charlson, R.J., Schwartz, S.E., Hales, J.M., Cess, R.D., Coakley Jr., J. A., Hansen, J.E., Hofmann, D.J., 1992. Climate forcing by anthropogenic aerosols. Science 255, 423–430.

Chin, M., Ginoux, P., Kinne, S., Torres, O., Holben, B.N., Duncan, B. N., Martin, R.V., Logan, J.A., Higurashi, A., Nakajima, T., 2002. Tropospheric aerosol optical thickness from the GOCART model and comparisons with satellite and sunphotometer measurements. J. Atmos. Sci. 59, 461–483.

Chin, M., Ginoux, P., Lucchesi, R., Huebert, B., Weber, R., Anderson, T., Masonis, S., Blomquist, B., Bandy, A., Thornton, D., 2003. A global aerosol model forecast for the ACE-Asia field experiment. J. Geophys. Res. 108 (D23), 8654. doi:10.1029/2003JD003642.

China National Committee for the Implementation of the United Nations Convention to Combat Desertification (CCICCD), 1997. China country paper to combat desertification. China Forestry Publishing House, Beijing, China.

Chung, S.H., Seinfeld, J.H., 2002. Global distribution and climate forcing of carbonaceous aerosols. J. Geophys. Res. 107, 4407. doi:10.1029/2001JD001397, 2002.

Clarke, A.D., Collins, W.G., Rasch, P.J., Kapustin, V.N., Moore, K., Howell, S., Fuelberg, H.E., 2001. Dust and pollution transport on global scales: aerosol measurements and model predictions. J. Geophys. Res. 106, 32,555–32,569.

Clarke, A.D., Shinozuka, Y., Kapustin, V.N., Howell, S., Huebert, B., Doherty, S., Anderson, T., Covert, D., Anderson, J., Hua, X., Moore II, K.G., McNaughton, C., Carmichael, G., Weber, R., 2004. Size distributions and mixtures of dust and black carbon aerosol in Asian outflow: physiochemistry and optical properties. J. Geophys. Res. 109, D15S09. doi:10.1029/2003JD004378.

Conant, W.C., Seinfeld, J.H., Wang, J., Carmichael, G.R., Tang, Y., Uno, I., Flatau, P.J., Markowicz, K.M., Quinn, P.K., 2003. A model for the radiative forcing during ACE-Asia derived from CIRPAS Twin Otter and R/V Ronald H. Brown data and comparison with observations. J. Geophys. Res. 108 (D23), 8661. doi:10.1029/2002JD003260.

DeFries, R.S., Townshend, J.R.G., 1994. NDVI-derived land cover classification at a global scale. Int. J. Remote Sens. 15, 3567–3586.

Doherty, S.J., Quinn, P., Jefferson, A., Carrico, C., Anderson, T.L., Hegg, D., 2005. A comparison and summary of aerosol optical properties as observed from aircraft, ship and land during ACE-Asia. J. Geophys. Res. 110, D04201. doi:10.1029/2004JD004964.

Dubovik, O., Holben, B.N., Lapyonok, T., Sinyuk, A., Mishchenko, M.I., Yang, P., Slutsker, I., 2002. Non-spherical aerosol retrieval method employing light scattering by spheroids. Geophys. Res. Lett. 29, 1415. doi:10.1029/2001GL014506.

Dubovik, O., Smirnov, A., Holben, B.N., King, M.D., Kaufman, Y.J., Eck, T.F., Slutsker, I., 2000. Accuracy assessments of aerosol optical properties retrieved from AERONET sun and sky-radiance measurements. J. Geophys. Res. 105, 9791–9806.

Gard, E., Mayer, J.E., Morrical, B.D., Dienes, T., Fergenson, D.P., Prather, K.A., 1997. Real-time analysis of individual atmospheric aerosol particles: design and performance of a portable ATOFMS. Anal. Chem. 69, 4083–4091.

Gard, E.E., Kleeman, M.J., Gross, D.S., Hughes, L.S., Allen, J.O., Morrical, B.D., Fergenson, D.P., Dienes, T., Galli, M.E., Johnson, R.J., Cass, G.R., Prather, K.A., 1998. Direct observation of heterogeneous chemistry in the atmosphere. Science 279, 1184–1187.

Ginoux, P., Chin, M., Tegen, I., Prospero, J.M., Holben, B., Dubovik, O., Lin, S.-J., 2001. Sources and global distributions of dust aerosols simulated with the GOCART model. J. Geophys. Res. 106, 20,255–20,273.

Gong, S.L., Zhang, X.Y., Zhao, T.L., McKendry, I.G., Jaffe, D.A., Lu, N.M., 2003. Characterization of soil dust aerosol in China and its transport and distribution during 2001 ACE-Asia: part 2 model simulation and validation. J. Geophys. Res. 108, 4262. doi:10.1029/2002JD002633.

Guazzotti, S.A., Coffee, K.R., Prather, K.A., 2001. Continuous measurements of size-resolved particle chemistry during INDOEX-intensive field phase 99. J. Geophys. Res. 106, 28607–28627.

Hanisch, F., Crowley, J.N., 2001. The heterogeneous reactivity of gaseous nitric acid on authentic mineral dust samples, and on individual mineral and clay mineral components. Phys. Chem. Chem. Phys. 3, 2474–2482.

Hess, M., Köpke, P., Schult, I., 1998. Optical properties of aerosols and clouds: the software package OPAC. Bull. Am. Meteorol. Soc. 79, 831–844.

Holden, C., 2001. The perfect dust storm, random samples. Science 294, 2469.

Höller, R., Ito, K., Tohno, S., Kasahara, M., 2003. Wavelength-dependent aerosol single-scattering albedo: measurements and model calculations for a coastal site near the Sea of Japan during ACE-Asia. J. Geophys. Res. 108 (D23), 8648. doi:10.1029/2002JD003250.

Hopke, P.K., Song, X.H., 1997. Classification of single particles by neural networks based on the computer-controlled scanning electron microscopy data. Anal. Chim. Acta 348, 375–388.

Howell, S.G., Clarke, A.D., Shinozuka, Y., Kapustin, V.N., McNaughton, C.S., Huebert, B.J., Doherty, S., Anderson, T., 2006. Influence of relative humidity upon pollution and dust during ACE-Asia: size distributions and implications for optical properties. J. Geophys. Res. 111, D06205. doi:10.1029/2004JD005759.

Huebert, B.J., Bates, T., Russell, P.B., Shi, G., Kim, Y.J., Kawamura, K., Carmichael, G., Nakajima, T., 2003. An overview of ACE-Asia: strategies for quantifying the relationships between Asian aerosols and their climatic impacts. J. Geophys. Res. 108 (D23), 8633. doi:10.1029/2003JD003550.

Huebert, B.J., Howell, S.G., Covert, D., Bertram, T., Clarke, A., Anderson, J.R., Lafleur, B.G., Seebaugh, W.R., Wilson, J.C.,

Gesler, D., Blomquist, B., Fox, J., 2004. PELTI: measuring the passing efficiency of an airborne low turbulence aerosol inlet. Aerosol Sci. Technol. 38, 803–826.

Intergovernmental Panel on Climate Change (IPCC), 1994. Radiative forcing of climate change. 1994 Report of the Intergovernmental Panel on Climate Change. Cambridge Univ. Press, New York, p. 139.

Jaffe, D., McKendry, I., Anderson, T., Price, H., 2003. Six 'new' episodes of trans-Pacific transport of air pollutants. Atmos. Environ. 37, 391–404.

Kalashnikova, O., Sokolik, I.N., 2004. Modeling optical properties of nonspherical soil-derived dust aggregates. J. Quant. Spectrosc. Radiat. Transfer 87, 137–166.

Kalashnikova, O.V., Kahn, R., Sokolik, I.N., Li, W.-H., 2005. The ability of multi-angle remote sensing observations to identify and distinguish mineral dust types: part 1. optical models and retrieval of optically thick plumes. J. Geophys. Res. 110, D18S14. doi:10.1029/2004JD004550.

Kim, Y.-P., Shim, S.-G., Moon, K.-C., 1998. Monitoring of air pollutants at Kosan, Cheju Island, Korea, during March–April 1994. J. Appl. Meteorol. 37, 1117–1126.

Kim, K.W., He, Z., Kim, Y.J., 2004. Physico-chemical characteristics and radiative properties of Asian dust particles observed at Kwangju, Korea, during the 2001 ACE-Asia IOP. J. Geophys. Res. 109 (D19S02). doi:10.1029/2003JD003693.

Kim, N.K., Kim, Y.P., Kang, C.H., Moon, K.C., 2004. Characteristics of nitrate concentration measured at Gosan, measurement data of PM2.5 and TSP between 1998 and 2002. J. Korean Soc. Atmos. Environ. 20, 119–128 (in Korean).

Kim, D.-H., Sohn, B.-J., Nakajima, T., Takamura, T., Takemura, T., Choi, B.-C., Yoon, S.-C, 2004. Aerosol optical properties over east Asia determined from ground-based sky radiation measurements. J. Geophys. Res. 109 (D02209). doi:10.1029/2003JD003387.

Kim, S.W., Yoon, S.C., Jefferson, A., Ogren, J.A., Dutton, E.G., Won, J.G., Ghim, Y.S., Lee, B.I., Han, J.S., 2005. Aerosol optical, chemical and physical properties at Gosan, Korea during Asian dust and pollution episodes in 2001. Atmos. Environ. 39, 39–50.

Kline, J., Huebert, B., Howell, S., Blomquist, B., Zhuang, J., Bertram, T., Carrillo, J., 2004. Aerosol composition and size versus altitude measured from the C-130 during ACE-Asia. J. Geophys. Res. 109 (D19). doi:10.1029/2004jd004540.

Krueger, B.J., Grassian, V.H., Cowin, J.P., Laskin, A., 2004. Heterogeneous chemistry of individual mineral dust particles from different dust source regions: the importance of particle mineralogy. Atmos. Environ. 38, 6253–6261.

Kwon, H.-J., Cho, S.-H., Chun, Y., Lagarde, F., Pershagan, G., 2002. Effects of the Asian dust events on daily mortality in Seoul, Korea. J. Environ. Res. 90 (A), 1–5.

Lafon, S., Rajot, J.L., Sokolik, I.N., Caquineau, S., Alfaro, S.C., Formenti, P., Maille, M., Gaudichet, A., 2004. Comprehensive characterization of size-resolved composition and morphology of mineral dust particles for radiative forcing studies. EOS Trans. AGU, Fall Meeting.

Lafon S., Sokolik, I.N., Rajot, J.L., Caquineau, S., Gaudichet, A, in press. Characterisation of iron oxides: implications to light absorption of mineral dust aerosols, J. Geophys. Res.

Lawson, D.R., Winchester, J.W., 1979. Sulfur, potassium and phospohorus associations in aerosols from South American tropical rain forests. J. Geophys. Res. 84, 3723–3727.

Lee, Y.-N., Weber, R.J., Ma, Y., Orsini, D., Maxwell, K., Blake, D., Meinardi, S., Sachse, G., Harward, C., Clarke, A.D., Moore, K., Kapustin, V.N., Chen, T.-Y., Thornton, D.C., Tu, F.H., Bandy, A. R., 2003. Airborne measurement of inorganic ionic components of fine aerosol particles using the PILS-IC technique during ACE-ASIA and TRACE-P. J. Geophys. Res. 108 (D23). doi:10.1029/2002JD003265.

Lee, K.H., Kim, Y.J., von Hoyningen-Huene, W., 2004. Estimation of aerosol optical thickness over northeast Asia from Sea-Viewing Wide Field-of-View (SeaWiFS) Sensor intensive observation period, data during the 2001 ACE-Asia intensive observation period. J. Geophys. Res. 109 (D19S16). doi:10.1029/2003JD004126.

Li, X., Maring, H.B., Savoie, D., Voss, K., Prospero, J.M., 1996. Dominance of mineral dust in aerosol light scattering in the North Atlantic trade winds. Nature 380, 416–419.

Liu, T., et al., 1985. Loess and the Environment. China Ocean Press, Beijing, People's Republic of China. 251 pp.

Liu, D.Y., Prather, K.A., Hering, S.V., 2000. Variations in the size and chemical composition of nitrate-containing particles in Riverside, CA. Aerosol Sci. Technol. 33 (1–2), 71–86.

Liu, M., Westphal, D.L., Wang, S., Shimizu, A., Sugimoto, N., Zhou, J., Chen, Y., 2003a. A high-resolution numerical study of the Asian dust storms of April 2001. J. Geophys. Res. 108 (D23), 8653. doi:10.1029/2002JD003178.

Liu, M., Westphal, D.L., Wang, S., Shimizu, A., Sugimoto, N., Zhou, J., Chen, Y., 2003b. A high-resolution numerical study of the Asian dust storms in April 2001. J. Geophys. Res. 108, 8653. doi:10.1029/2002JD003178.

Marticorena, B., Bergametti, G., 1995. Modelling the atmospheric dust cycle: 1. Design of a soil-derived dust emission scheme. J. Geophys. Res. 100, 16,415–16,430.

Maxwell-Meier, K.L., Weber, R., Orsini, D., Ma, Y., Carmichael, G., Streets, D., 2004. Inorganic Composition of particles in mixed dust — pollution plumes observed from airborne measurements during ACE -ASIA. J. Geophys. Res. 109 (D19S07). doi:10.1029/2003JD004464.

Mishchenko, M.I., Travis, L.D., 2003. Electromagnetic scattering by nonspherical particles. In: Guzzi, R. (Ed.), Exploring the Atmosphere by Remote Sensing Techniques. Springer-Verlag, Berlin, pp. 77–127.

Murayama, T., Masonis, S.J., Redemann, J., Anderson, T.L., Schmid, B., Livingston, J.M., Russell, P.B., Huebert, B., Howell, S.G., McNaughton, C.S., Clarke, A., Abo, M., Shimizu, A., Sugimoto, N., Yabuki, M., Kuze, H., Fukagawa, S., Maxwell-Meier, K.L., Weber, R.J., Orsini, D.A., Blomquist, B., Bandy, A., Thornton, D., 2003. An intercomparison of lidar-derived optical properties with airborne measurements near Tokyo during ACE-Asia. J. Geophys. Res. 108 (D23), 8651. doi:10.1029/2002JD003259, 2003.

Natsagdorj, L., Jugder, D., Chung, Y.S., 2003. Analysis of dust storms observed in Mongolia during 1937–1999. Atmos. Environ. 37, 1401–1411.

Noble, C.A., Prather, K.A., 1996. Real-time measurement of correlated size and composition profiles of individual atmospheric aerosol particles. Environ. Sci. Technol. 30, 2667–2680.

Nriagu, J.O., Pacyna, J.M., 1988. Quantitative assessment of worldwide contamination of air, water and soils by trace metals. Nature 333, 134–139.

Ogunjobi, K.O., He, Z., Kim, K.W., Kim, Y.J., 2004. Aerosol optical depth during episodes of Asian dust storms and biomass burning at Kwangju, South Korea. Atmos. Environ. 38, 1313–1323.

Park, M.H., Kim, Y.P., Kang, C.-H., 2003. Aerosol composition change due to dust storm: measurements between 1992 and 1999 at Gosan, Korea. Water Air Soil Pollut. Focus 3, 117–128.

Park, M.H., Kim, Y.P., Kang, C.-H., Shim, S.-G., 2004. Aerosol composition change between 1992 and 2002 at Gosan, Korea. J. Geophys. Res. 109 (D19S13). doi:10.1029/2003JD004110.

Patterson, E.M., Gillete, D.A., Stockton, B.H., 1977. Complex index of refraction between 300 and 700 nm for Saharan aerosol. J. Geophys. Res. 82, 3153–3160.

Perry, K.D., Cahill, T.A., Eldred, R.A., Dutcher, D.D., Gill, T.E., 1997. Long-range transport of North African dust to the eastern United States. J. Geophys. Res. 102, 11,225–11,238.

Porter, S.C., 2001. Chinese loess record of monsoon climate during the last glacial–interglacial cycle. Earth Sci. Rev. 54, 115–128.

Prather, K.A., Nordmeyer, T., Salt, K., 1994. Real-time characterization of individual aerosol particles using time-of-flight mass spectrometry. Anal. Chem. 66, 1403–1407.

Quinn, P.K., Coffman, D.J., Bates, T.S., Welton, E.J., Covert, D.S., Miller, T.L., Johnson, J.E., Maria, S., Russell, L., Arimoto, R., Carrico, C.M., Rood, M.J., Anderson, J., 2004. Aerosol optical properties measured onboard the Ronald H. Brown during ACE Asia as a function of aerosol chemical composition and source region. J. Geophys. Res. 109 (D19S01). doi:10.1029/2003JD004010.

Raabe, O.G., Braaten, D.A., Axelbaum, R.L., Teague, S.V., Cahill, T. A., 1988. Calibration studies of the drum impactor. J. Aerosol Sci. 19, 183–195.

Redemann, J., Masonis, S.J., Schmid, B., Anderson, T.L., Russell, P., Livingston, J., Dubovik, O., Clarke, A., 2003. Clear-column closure studies of aerosol and water vapor aboard the NCAR C-130 during ACE-Asia, 2001. J. Geophys. Res. 108 (D23), 8655. doi:10.1029/2003JD003442.

Reid, J.S., Jonsson, H.H., Maring, H.B., Smirnov, A., Savoie, D.L., Cliff, S.S., Reid, E.A., Livingston, J.M., Meier, M.M., Dubovik, O., Tsay, S.-C., 2003. Comparison of size and morphological measurements of coarse mode dust particles from Africa. J. Geophys. Res. 108 (D19), 8591. doi:10.1029/2002JD002935.

Ryu, S.Y., Kim, J.E., Zhuanshi, H., Kim, Y.J., Kang, G.U., 2004. Chemical composition of post-harvest biomass burning aerosols in Gwangju, Korea. J. Air Waste Manage. Assoc. 54, 1124–1137.

Seinfeld, J.H., Carmichael, G.R., Arimoto, R., Conant, W.C., Brechtel, F.J., Bates, T.S., Cahill, T.A., Clarke, A.D., Doherty, S.J., Flatau, P. J., Huebert, B.J., Kim, J., Markowicz, K.M., Quinn, P.K., Russell, L.M., Russell, P.B., Shimizu, A., Shinozuka, Y., Song, C.H., Tang, Y., Uno, I., Vogelmann, A.M., Weber, R.J., Woo, J-H., Zhang, X. Y., 2004. ACE-ASIA: regional climatic and atmospheric chemical effects of Asian dust and pollution. Bull. Am. Meteorol. Soc. 85, 367–380.

Shi, A., Shao, L., Jones, T.P., Whittaker, A.G., Lu, S., Bérubé, K.A., He, T., Richards, R.J., 2003. Characterization of airborne individual particles collected in an urban area, a satellite city and a clear air area in Beijing, 2001. Atmos. Environ. 37, 4097–4108.

Shimizu, A., Sugimoto, N., Matsui, I., Arao, K., Uno, I., Murayama, T., Kagawa, N., Aoki, K., Uchiyama, A., Yamazaki, A., 2004. Continuous observations of Asian dust and other aerosols by polarization lidars in China and Japan during ACE-Asia. J. Geophys. Res. 109 (D19S17). doi:10.1029/2002JD003253.

Silva, P.J., Liu, D.Y., Noble, C.A., Prather, K.A., 1999. Size and chemical characterization of individual particles resulting from biomass burning of local Southern California species. Environ. Sci. Technol. 33, 3068–3076.

Sokolik, I.N., Winker, D.M., Bergametti, G., Gillette, D.A., Carmichael, G., Kaufman, Y.J., Gomes, L., Schuetz, L., Penner, J.E., 2001. Introduction to special section: outstanding problems in quantifying the radiative impacts of mineral dust. J. Geophys. Res. 106, 18,015–18,027.

Sokolik, I.N., Anderson, J., Guazzotti, S.A., Prather, K.A., 2003. New techniques for predicting optical properties of nonspherical multicomponent aerosols using single particle measurements. EOS Trans. AGU, Fall Meeting. .

Song, C.H., Carmichael, G.R., 2001. Gas-particle partitioning of nitric acid modulated by alkaline aerosol. J. Atmos. Chem. 40, 1–22.

Song, X.H., Hopke, P.K., Fergenson, D.P., Prather, K.A., 1999. Classification of single particles analyzed by ATOFMS using an artificial neural network, ART-2A. Anal. Chem. 71, 860–865.

Sullivan, R.C., Guazzotti, S.A., Sodeman, D.A., Prather, K.A., in press. Direct observations of the atmospheric processing of Asian mineral dust. Atmos Chem. Phys. Discuss.

Sun, J., Zhang, M., Liu, T., 2001. Spatial and temporal characteristics of dust storms in China and its surrounding regions, 1960–1999: relations to source area and climate. J. Geophys. Res. 106, 10,325–10,333.

Takemura, T., Nakajima, T., Higurashi, A., Ohta, S., Sugimoto, N., 2003. Aerosol distributions and radiative forcing over the Asian Pacific region simulated by Spectral Radiation-Transport Model for Aerosol Species (SPRINTARS). J. Geophys. Res. 108 (D23), 8659. doi:10.1029/2002JD003210.

Tang, U., Carmichael, G.R., Seinfeld, J.H., Dabdub, D., Weber, R.J., Huebert, B., Clarke, A.D., Guazzotti, S.A., Prather, K.A., Uno, I., Woo, J.-H., Streets, D.G., Quinn, P., Johnson, J.E., Song, C.-H., Sandu, A., Talbot, R.W., Dibb, J.E., 2004a. Three-dimensional simulations of inorganic aerosol distributions in east Asia during spring 2001. J. Geophys. Res. 109 (D19), D19S23. doi:10.1029/2003JD004201.

Tang, Y., Carmichael, G.R., Kurata, G., Uno, I., Weber, R., Song, C.H., Guttikunda, S.K., Woo, J.H., Streets, D.G., Wei, C., Clarke, A.D., Huebert, B., Anderson, T.L., 2004b. Impacts of dust on regional tropospheric chemistry during the ACE-Asia experiment: a model study with observations. J. Geophys. Res. 109 (D19S21). doi:10.1029/2003JD003806.

Taylor, S.R., McLennan, S.M., 1995. The geochemical evolution of the continental crust. Rev. Geophys. 33, 241–265.

Uematsu, M., Duce, R.A., Prospero, J.M., 1985. Deposition of atmospheric mineral particles in the North Pacific Ocean. J. Atmos. Chem. 3, 123–138.

Uematsu, M., Yoshikawa, A., Muraki, H., Arao, K., Uno, I., 2002. Transport of mineral and anthropogenic aerosols during a Kosa event over East Asia. J. Geophys. Res. 107 (D7). doi:10.1029/2001JD000333, 2002.

Uno, I., et al., 2003. Regional chemical weather forecasting system CFORS: model descriptions and analysis of surface observations at Japanese island stations during the ACE-Asia experiment. J. Geophys. Res. 108 (D23), 8668. doi:10.1029/2002JD002845.

Uno, I., Satake, S., Carmichael, G.R., Tang, Y., Wang, Z., Takemura, T., Sugimoto, N., Shimizu, A., Murayama, T., Cahill, T.A., Cliff, S., Uematsu, M., Ohta, S., Quinn, P.K., Bates, T.S., 2004. Numerical Study of Asia Dust Transport during the Springtime of 2001 simulated with the CFORS model. J. Geophys. Res. 109 (D19), D19S24. doi:10.1029/2003JD004222.

Usher, C.R., Michel, A.E., Grassian, V.H., 2003. Reactions on mineral dust. Chem. Rev. 103, 4883–4939.

VanCuren, R.A., Cahill, T.A., 2002. Asian aerosols in North America: frequency and concentration of fine dust. J. Geophys. Res. 107. doi:10.1029/2002JD002204.

Wang, J., Christopher, S.A., Brechtel, F.J., Kim, J., Schmid, B., Redemann, J., Russell, P.B., Quinn, P.K., Holben, B., 2003. Geostationary satellite retrievals of aerosol optical thickness during ACE-Asia. J. Geophys. Res. 108 (D23), 8657. doi:10.1029/2003JD003580.

Wurzler, S., Reisin, T.G., Levin, Z., 2000. Modification of mineral dust particles by cloud processing and subsequent effects on drop size distributions. J. Geophys. Res. 105, 4501–4512.

Xie, Y., Hopke, P.K., Wienke, D., 1994. Airborne particle classification with a combination of chemical composition and shape index utilizing an adaptive resonance artificial neural network. Environ. Sci. Technol. 28, 1921–1928.

Xu, J., Bergin, M.H., Greenwald, R., Schauer, J.J., Shafer, M.M., Jaffrezo, J.L., Aymoz, G., 2004. Aerosol chemical, physical, and radiative characteristics near a desert source region of northwest China during ACE-Asia. J. Geophys. Res. 109 (D19S03). doi:10.1029/2003JD004239.

Zender, C.S., Miller, R.L., Tegen, I., 2004. Quantifying mineral dust mass budgets: terminology, constraints, and current estimates. EOS, Trans., Amer. Geophys. Union 85, 509–512.

Zhang, D., 1984. Synoptic–climatic studies of dust fall in China since historic times. Sci. Sin., Ser. B, Chem. Biol. Agric. Med. Earth Sci. 27, 825–836.

Zhang, X., Arimoto, R., An, Z., Chen, T., Zhang, G., Shu, G., Wang, X., 1993. Atmospheric trace elements over source regions of Chinese dust: concentrations, sources and atmospheric input to the Loess Plateau. Atmos. Environ. 27A, 2051–2067.

Zhang, X.Y., Arimoto, R., Zhu, G.H., Chen, T., Zhang, G.Y., 1998. Concentration, size-distribution and deposition of mineral aerosol over Chinese desert regions. Tellus 50B, 317–330.

Zhang, X.Y., Arimoto, R., An, Z.S., Cao, J.J., Wang, D., 2001. Atmospheric dust aerosol over the Tibetian Plateau. J. Geophys. Res. 106, 18,471–18,476.

Zhang, X.Y., Gong, S.L., Zhao, T.L., Arimoto, R., Wang, Y.Q., Zhou, Z.J., 2003a. Sources of Asian dust and role of climate change versus desertification in Asian dust emission. Geophys. Res. Lett. 30, 2272. doi:10.1029/2003GL018206.

Zhang, X.Y., Gong, S.L., Arimoto, R., Shen, Z.X., Mei, F.M., Wang, D., Cheng, Y., 2003b. Characterization and temporal variation of Asian dust aerosol from a site in the northern Chinese deserts. J. Atmos. Chem. 44, 241–257.

Zhao, T.L., Gong, S.L., Zhang, X.Y., McKendry, I.G., 2003. Modelled size-segregated wet and dry deposition budgets of soil dust aerosol during ACE-Asia, 2001: implications for Trans-Pacific transport. J. Geophys. Res. 108 (D23), 8665. doi:10.1029/2002JD003363.